



Mistry, Shailesh N. and Drinkwater, Nyssa and Ruggeri, Chiara and Sivaraman, Komagal Kannan and Loganathan, Sasdekumar and Fletcher, Sabine and Drag, Marcin and Paiardini, Alessandro and Avery, Vicky M. and Scammells, Peter J. and McGowan, Sheena (2014) Two-pronged attack: dual inhibition of Plasmodium falciparum M1 and M17 metalloaminopeptidases by a novel series of hydroxamic acid-based inhibitors. *Journal of Medicinal Chemistry*, 57 (21). pp. 9168-9183. ISSN 0022-2623

Access from the University of Nottingham repository:

<http://eprints.nottingham.ac.uk/30418/1/9A502CEF-1A0E-4F8A-866E-FE51E2B7984D.pdf>

Copyright and reuse:

The Nottingham ePrints service makes this work by researchers of the University of Nottingham available open access under the following conditions.

- Copyright and all moral rights to the version of the paper presented here belong to the individual author(s) and/or other copyright owners.
- To the extent reasonable and practicable the material made available in Nottingham ePrints has been checked for eligibility before being made available.
- Copies of full items can be used for personal research or study, educational, or not-for-profit purposes without prior permission or charge provided that the authors, title and full bibliographic details are credited, a hyperlink and/or URL is given for the original metadata page and the content is not changed in any way.
- Quotations or similar reproductions must be sufficiently acknowledged.

Please see our full end user licence at:

http://eprints.nottingham.ac.uk/end_user_agreement.pdf

A note on versions:

The version presented here may differ from the published version or from the version of record. If you wish to cite this item you are advised to consult the publisher's version. Please see the repository url above for details on accessing the published version and note that access may require a subscription.

For more information, please contact eprints@nottingham.ac.uk

Two-Pronged Attack: Dual Inhibition of *Plasmodium falciparum* M1 and M17 Metalloaminopeptidases by a Novel Series of Hydroxamic Acid-Based Inhibitors

Shailesh N. Mistry,^{†,‡} Nyssa Drinkwater,^{‡,§} Chiara Ruggeri,^{‡,§} Komagal Kannan Sivaraman,[‡] Sasdekumar Loganathan,^{||} Sabine Fletcher,^{||} Marcin Drag,[⊥] Alessandro Paiardini,[§] Vicky M. Avery,^{||} Peter J. Scammells,^{*,†} and Sheena McGowan^{*,‡}

[†]Medicinal Chemistry, Monash Institute of Pharmaceutical Sciences, Monash University, Parkville, Victoria 3052, Australia

[‡]Department of Biochemistry and Molecular Biology, Monash University, Clayton, Victoria 3800, Australia

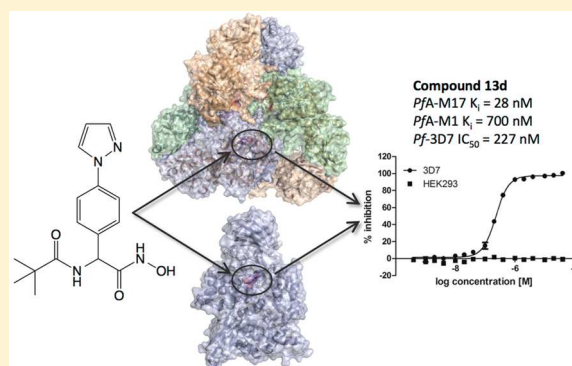
[§]Dipartimento di Scienze Biochimiche "A. Rossi Fanelli", Sapienza Università di Roma, 00185 Roma, Italy

^{||}Discovery Biology, Eskitis Institute for Drug Discovery, Griffith University, Nathan, Queensland 4111, Australia

[⊥]Division of Bioorganic Chemistry, Faculty of Chemistry, Wrocław University of Technology, Wyb. Wyspińskiego 27, 50-370 Wrocław, Poland

S Supporting Information

ABSTRACT: *Plasmodium* parasites, the causative agents of malaria, have developed resistance to most of our current antimalarial therapies, including artemisinin combination therapies which are widely described as our last line of defense. Antimalarial agents with a novel mode of action are urgently required. Two *Plasmodium falciparum* aminopeptidases, *PfA*-M1 and *PfA*-M17, play crucial roles in the erythrocytic stage of infection and have been validated as potential antimalarial targets. Using compound-bound crystal structures of both enzymes, we have used a structure-guided approach to develop a novel series of inhibitors capable of potent inhibition of both *PfA*-M1 and *PfA*-M17 activity and parasite growth in culture. Herein we describe the design, synthesis, and evaluation of a series of hydroxamic acid-based inhibitors and demonstrate the compounds to be exciting new leads for the development of novel antimalarial therapeutics.



INTRODUCTION

Malaria, caused by parasites of the genus *Plasmodium* (of which *Plasmodium falciparum*, *Pf*, is the most lethal), is the world's most prevalent parasitic disease. The spread of drug-resistant parasites has rendered most of the current antimalarial treatments ineffective; consequently, prevention and treatment of malaria is becoming increasingly difficult. The most recent WHO World Malaria Report indicated that, in 2012 alone, there were approximately 627 000 deaths from malaria. There is an urgent need for next-generation antimalarial agents with novel modes of action.

During the symptomatic erythrocytic stage of *Pf* infection, parasites degrade hemoglobin into free amino acids.^{1,2} These free amino acids are essential in a variety of critical processes, including parasite growth and development,² protein synthesis, and maintenance of osmotic pressure within the infected red blood cell to prevent premature cell lysis.³ The final stage of hemoglobin digestion is mediated by metalloaminopeptidases (MAPs), which act to degrade small peptide fragments into free amino acids.^{4,5} Inhibitors of these enzymes thus represent

attractive leads for the development of novel antimalarial therapeutic agents. *Pf* employs two neutral MAPs, *PfA*-M1 and *PfA*-M17. Both enzymes bear zinc-binding motifs that have essential roles in both substrate and inhibitor binding.⁶

Inhibition of *PfA*-M1 and *PfA*-M17 has been shown to control both *Pf* laboratory and *Plasmodium chabaudi chabaudi* murine models of malaria,^{7,8} and while potent inhibitors of either *PfA*-M1 or *PfA*-M17 have been identified,^{7–12} differences in the compound binding profiles of the enzymes mean that compound elaboration generally favors selectivity for one enzyme over the other. Previous work within our group identified ((4-(1*H*-pyrazol-1-yl)phenyl)aminomethyl)-phosphonic acid (**1**) (Figure 1) as a lead for the development of a dual inhibitor of both *PfA*-M1 and *PfA*-M17.¹³ X-ray crystal structures of both enzymes in complex with **1** showed that the compound sits within the S1 pocket and coordinates the catalytic zinc ion(s) through the aminophosphonate moiety.¹³

Received: August 28, 2014

Published: October 9, 2014

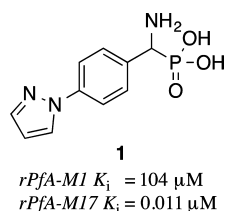


Figure 1. ((4-(1*H*-Pyrazol-1-yl)phenyl)aminomethyl)phosphonic acid (**1**).¹³

Although aminophosphonates are an established zinc-binding group (ZBG), the phosphonic acid group would exist as a dianion at physiological pH ($pK_a = 2.35$ and ~ 6)¹⁴ with potentially detrimental effects on membrane permeability. To generate dual *PfA*-M1/*PfA*-M17 inhibitors and address potential permeability issues conferred by the aminophosphonate moiety, we sought to employ an alternative ZBG. Hydroxamic acid-based compounds that are capable of reaching the site of action within infected red blood cells and inhibiting *PfA*-M1 have been described previously.¹⁰ Therefore, we replaced the phosphonic acid moiety of **1** with a hydroxamic acid to generate compounds that would have a more desirable permeability^{15,16} and plasma stability profile.¹⁷ The hydroxamic acid group has been successfully used in inhibitors for several proteases, the most attractive being tosedostat, which shows promising efficacy in phase II clinical trials for patients with myelodysplastic syndrome and/or acute myeloid leukemia.¹⁸ Herein, we report the design, synthesis, and inhibitory activity of novel carboxylic and hydroxamic acid derivatives of **1**, leading to the discovery of compound **7** as a potent dual inhibitor of *PfA*-M1/*PfA*-M17. Utilizing compound **7** as our new lead, we investigated structure–activity relationships (SARs) of this scaffold further through a series of *N*-acyl derivatives in replacement of the *N*-Boc group. Finally, we demonstrate parasitocidal activity of our more potent dual inhibitors.

RESULTS AND DISCUSSION

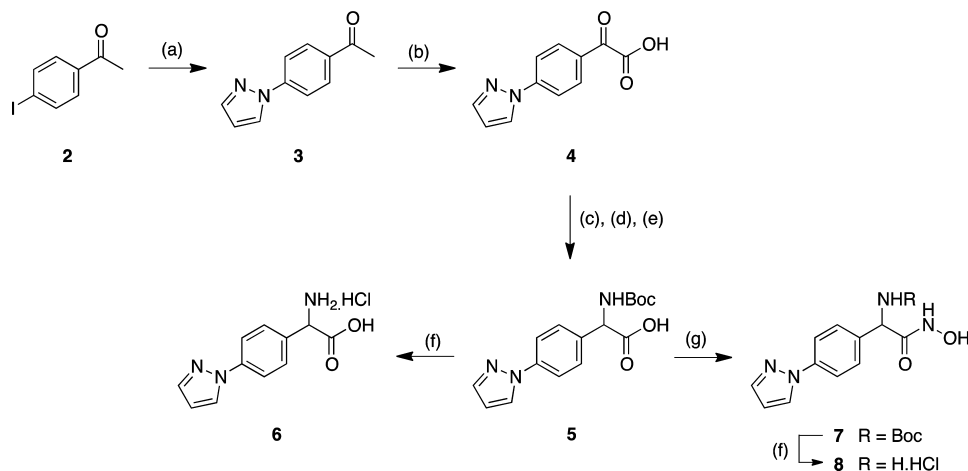
Chemistry. It was envisaged that the desired α -amino-hydroxamic acid functionality could be accessed from the

corresponding *N*-Boc-protected amino acid by first coupling with hydroxylamine before *N*-Boc deprotection to unmask the final compound. Our initial strategy employed 2-amino-2-(4-bromophenyl)acetic acid as a starting material. *N*-Boc protection of the amine and esterification of the carboxylic acid functionality were performed, prior to attempted Ullmann-type coupling with pyrazole under a variety of conditions,^{19–21} none of which were successful (data not shown). Suspecting the presence of the bulky protected amine and carboxylic acid groups to be responsible for the failed coupling (through either a steric or a potentially catalyst-chelating mechanism), an alternative strategy was devised, whereby Ullman-type *N*-arylation of pyrazole could be carried out with a simple coupling partner, with subsequent installation of the α -amino acid functionality (Scheme 1).

Literature precedent for the synthesis of 1-(4-(1*H*-pyrazol-1-yl)phenyl)ethan-1-one (**3**) in good to excellent yield is widespread.^{22–33} In our hands, *N*-arylation of pyrazole with 4'-iodoacetophenone (**2**) to give **3** was achieved in near-quantitative yield using copper(I)-catalyzed, ligand-free Ullmann-type coupling.²¹ Subsequent oxidation of **3** to the corresponding α -keto acid **4** was achieved with ease, using SeO_2 /pyridine as the oxidation system.³⁴ Installation of the racemic amino acid system was carried out through initial reductive amination of the ketone moiety of **4** with *N,N*-dibenzylamine and $Na(OAc)_3BH$ under standard conditions.³⁵ The intermediate *N,N*-dibenzyl-protected amino acid then underwent complete debenzylation in the presence of 10% Pd/C in acidified methanol under a hydrogen atmosphere. Finally, *N*-Boc protection of the HCl salt of the intermediate amino acid was carried out using Boc_2O under mildly basic conditions. After purification, 2-(4-(1*H*-pyrazol-1-yl)phenyl)-2-((*tert*-butoxycarbonyl)amino)acetic acid (**5**) was obtained in 56% yield over three steps.

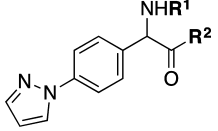
The hydroxamic acid ZBG has commonly been derived from the corresponding carboxylic acid precursor. In many cases the carboxylic acid group has also been found to possess the ability to bind zinc ions, albeit generally more weakly than the corresponding hydroxamic acid.^{15,16} With this in mind, we chose to evaluate the inhibitory activity of both the carboxylic

Scheme 1. Synthesis of Carbonyl Derivatives of ((4-(1*H*-Pyrazol-1-yl)phenyl)aminomethyl)phosphonic Acid (**1**)^a



^aReagents and conditions: (a) pyrazole, CS_2CO_3 , Cu_2O , DMF, 100 °C, 97%; (b) SeO_2 , anhydrous pyridine, 110 °C, 92%; (c) *N,N*-dibenzylamine, $Na(OAc)_3BH$, 1,2-dichloroethane, rt; (d) H_2 , 10% Pd/C, concd HCl, MeOH, water, rt; (e) $NaHCO_3(aq)$, Boc_2O , THF, rt, 56% (over three steps); (f) 4 M HCl/1,4-dioxane, DCM, rt, 25–97%; (g) (i) CDI, THF, rt; (ii) $NH_2OH \cdot HCl$, rt, 69%.

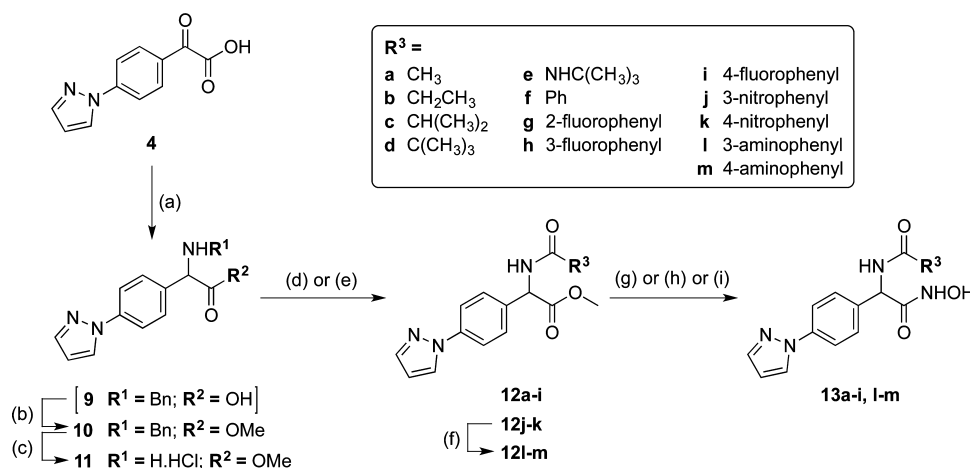
Table 1. Inhibition of PfA-M1 and PfA-M17 by Novel Hydroxamic Acid Derivatives 5–8 and 13a–m



	R ¹	R ²	K _i ^a (μM)		IC ₅₀ ± SD ^b (nM)
			rPfA-M1	rPfA-M17	
5	Boc	OH	>500	464	
6	H·HCl	OH	>500	>500	
7	Boc	NHOH	0.8	0.03	783 ± 86.6
8	H·HCl	NHOH	74.5	86	
13a	CH ₃ (C=O)	NHOH	113	0.019	619 ± 52.7
13b	CH ₃ CH ₂ (C=O)	NHOH	41.3	0.016	455 ± 60.9
13c	(CH ₃) ₂ CH(C=O)	NHOH	12.3	0.053	532 ± 13.3
13d	^t Bu(C=O)	NHOH	0.7	0.028	227 ± 4.24
13e	^t BuNH(C=O)	NHOH	15.3	0.038	597 ± 10.2
13f	benzoyl	NHOH	23	0.154	
13g	2-fluorobenzoyl	NHOH	1.9	0.008	351 ± 29.8
13h	3-fluorobenzoyl	NHOH	4	0.035	429 ± 30.6
13i	4-fluorobenzoyl	NHOH	11.2	0.012	703 ± 49.8
13l	3-aminobenzoyl	NHOH	5.5	0.014	233 ± 124.8
13m	4-aminobenzoyl	NHOH	7.4	0.011	228 ± 23.47

^aK_i values were calculated using Dixon plots of 1/V versus inhibitor concentration while the substrate concentration was maintained lower than that of the K_m of the enzyme. Dixon plots can be found in Supplementary Figure 1 (Supporting Information). ^bIC₅₀ values were calculated against *P. falciparum* 3D7. See also Supplementary Figure 6 (Supporting Information).

Scheme 2. Synthesis of Amide and Urea Analogues of *tert*-Butyl (1-(4-(1*H*-Pyrazol-1-yl)phenyl)-2-(hydroxyamino)-2-oxoethyl)carbamate (7)^a



^aReagents and conditions: (a) (i) benzylamine, anhydrous 1,2-dichloroethane, rt; (ii) Na(OAc)₃BH, rt, 76%; (b) concd H₂SO₄, MeOH, reflux, 89%; (c) (i) H₂ (balloon), 10% Pd/C, concd HCl, MeOH; (ii) satd NaHCO₃ workup; (iii) 1 M HCl/Et₂O, Et₂O, DCM, 87%; (d) (i) TEA, DCM; (ii) acid chloride or isocyanate, 85–99%; (e) substituted benzoic acid, HCTU, DIPEA, DCM, DMF, rt, 100%; (f) 10% Pd/C, MeOH, rt, 91–97%; (g) (i) NH₂OH·HCl, MeOH, rt; (ii) KOH/MeOH, 35–68%; (h) (i) NH₂OH·HCl, MeOH, rt; (ii) KOH/MeOH; (iii) FCC purification to isolated acid; (iv) CDI, dry THF, rt; (v) NH₂OH·HCl, 4–8%; (i) (i) dry MeOH, rt; (ii) NH₂OH·HCl, 5 M KOH/MeOH, dry MeOH (premixed), 43–47%.

acid and hydroxamic acid derivatives of **1**. *N*-Boc deprotection of **5** in the presence of 4 M HCl/dioxane and DCM afforded the HCl salt of the α -aminocarboxylic acid derivative **6** in near-quantitative yield. In contrast, the desired hydroxamic acid derivative was accessed via a two-step procedure. Initial conversion of *N*-Boc-protected α -aminocarboxylic acid **5** to the corresponding *N*-Boc-protected α -aminohydroxamic acid **7** was achieved in good yield by CDI-mediated activation followed by condensation with NH₂OH·HCl under the

reported conditions.³⁶ Finally, the desired α -aminohydroxamic acid **8** was obtained in the HCl salt form through *N*-Boc deprotection of **7**.

Evaluation of the inhibitory activity of **5**–**8** against PfA-M1 and PfA-M17 revealed *N*-Boc-protected α -aminohydroxamic acid **7** to be a potent, submicromolar inhibitor of both enzymes (Table 1). We were therefore curious to investigate the effect that other moieties would have at this position. To this end, we developed a series of *N*-acyl derivatives, based on **7**, comprised

of simple linear and branched alkyl groups as well as substituted aryl moieties. Access to these compounds was achieved from the previously synthesized compound **4** in five to six steps (Scheme 2).

As described above, α -keto acid **4** underwent reductive amination with benzylamine rather than *N,N*-dibenzylamine to improve the rate and reaction outcome (the corresponding reaction with *N,N*-dibenzylamine proceeded slowly, and complete conversion was not achieved). The new conditions were successful, and the reaction was complete after overnight stirring, generating the *N*-benzylamino acid **9** in good yield. This was subsequently esterified with MeOH in the presence of catalytic concentrated $\text{H}_2\text{SO}_4(\text{aq})$ to give the corresponding methyl ester **10**. Attempts to obtain **10** through a reversal of the reaction sequence (i.e., esterification followed by reductive amination) proved unsuccessful. Heating **4** under the esterification conditions described above resulted in both methyl ester formation and conversion of the ketone to the corresponding dimethyl ketal. Although selective deprotection of the ketal was achieved by allowing it to stand in TFA,³⁷ attempted reductive amination of the resulting α -keto ester produced several side products by LC/MS analysis, including the ketone **3**, the α -keto alcohol (total reduction of the ester), the α -hydroxy ester (ketone reduction), and the *N*-benzylamino acid **9**.

N-Debenzylation of **10** was achieved as described under acidic hydrogenation conditions in excellent yield, affording α -amino ester **11** as the HCl salt. Compound **11** underwent acylation with a selection of alkyl and substituted benzoyl chlorides, benzoic acids, and *tert*-butyl isocyanate. Where an acid chloride or *tert*-butyl isocyanate was used as the electrophile, it was simply stirred with **11** in the presence of a slight excess of TEA to give the corresponding amide or urea in excellent yield, with only aqueous workup required to isolate the desired product cleanly. Coupling to substituted benzoic acids was achieved in the presence of HCTU/DIPEA in DMF at room temperature, once again with only simple aqueous workup necessary to afford high-purity amide product. The nitrobenzamides **12j–k** were reduced to the corresponding aminobenzamides over 10% Pd/C in MeOH under a hydrogen atmosphere in excellent yield.

Evaluation of the literature indicated successful aminolysis of simple esters on similar scaffolds with $\text{NH}_2\text{OH}\cdot\text{HCl}$ directly.^{38–44} Such a conversion is attractive as it removes the need to hydrolyze the ester prior to a coupling step. After conducting successful pilot reactions, we opted to employ the combination of $\text{NH}_2\text{OH}\cdot\text{HCl}$ and methanolic KOH.⁴³ These conditions gave mixed results for the conversion of methyl esters **12a–i** and **12l–m** to the corresponding hydroxamic acids. Following the literature procedure, we obtained the desired compounds in modest yield in the majority of cases, with the remainder of reactions affording the corresponding carboxylic acid (through basic hydrolysis) as the major product. Even in cases where the desired hydroxamic acid was successfully isolated, generation of the carboxylic acid product was also noted. Where only the carboxylic product was isolated, this was converted to the corresponding hydroxamic acid product using CDI-mediated activation as described earlier in the synthesis of **7**.

Further optimization of the aminolysis conditions allowed more consistent conversion to the desired hydroxamic acid product, with a lower proportion of hydrolysis to the carboxylic acid being observed by LC/MS analysis. These conditions

involved the use of anhydrous MeOH as the reaction solvent and to make up the methanolic KOH solution. In addition, the KOH stock solution was stored under a septum under an atmosphere of nitrogen to exclude exposure to moisture. Finally, rather than sequential addition of $\text{NH}_2\text{OH}\cdot\text{HCl}$ and methanolic KOH, the two were premixed before addition to the appropriate ester reagent. This was done with a view to freshly generate the free NH_2OH nucleophile prior to addition, thus reducing the concentration of circulating hydroxide ions and reducing the risk of ester hydrolysis.

The Hydroxamic Acid Compound Series Probes the S1' Cavity of PfA-M1 and PfA-M17. In synthesizing **8**, the aminohydroxamic acid analogue of aminophosphonic acid **1**, we identified **7**, the *N*-Boc precursor of **8**, as a potent inhibitor of both *PfA*-M1 and *PfA*-M17 (Table 1; Supplementary Figure 1, Supporting Information). The *PfA*-M1 inhibitory activity of **7** ($K_i = 0.8 \mu\text{M}$) is approximately 100-fold higher than that of **1** ($K_i = 104 \mu\text{M}$), while the *PfA*-M17 activities are comparable (the K_i of **1** is $0.011 \mu\text{M}$, and that of **7** is $0.03 \mu\text{M}$), making **7** the most potent dual *PfA*-M1/M17 inhibitor described to date. To assess the selectivity of **7** for *PfA*-M1 and *PfA*-M17 over other MAPs, the inhibitory activity against *PfM18AAP*, another *P. falciparum* MAP,⁴⁵ was determined. The observed K_i for *PfM18AAP*, $49.6 \mu\text{M}$, showed that **7** is >60-fold and 1600-fold selective for *PfA*-M1 and *PfA*-M17, respectively. To investigate the structural mechanism behind the improved *PfA*-M1 and *PfA*-M17 potency, we determined the cocrystal structure of compound **7** bound to *PfA*-M1 (*PfA*-M1:7) and *PfA*-M17 (*PfA*-M17:7). Similarly to **1**, compound **7** coordinates strongly to the catalytic zinc ion(s) of both *PfA*-M1 and *PfA*-M17 and probes the hydrophobic S1 pocket with the aromatic regions of the compound (namely, a 4-(1*H*-pyrazol-1-yl)phenyl moiety). However, the *N*-Boc group, which is not present on **1**, was observed binding within the S1' cavity. Since the S1' cavity has not previously been explored with this series of inhibitors, we chose to probe the region with a focused library of *N*-acyl derivatives, assessing dual *PfA*-M1/M17 inhibitory activity and using structural information obtained from a combination of X-ray crystallography and docking analysis to guide inhibitor development.

The crystal structures of *PfA*-M1 and *PfA*-M17 bound to selected compounds in the series were determined by either cocrystallization or soaking experiments. Similarly to previous ligand-bound *PfA*-M1 and *PfA*-M17 crystal structures, the only structural differences observed on compound binding occurred within proximity of the active sites, while the overall protein folds and domain arrangements were unchanged. In all structures, *PfA*-M1 crystallized as a monomer, with one copy in the asymmetric unit. In accordance with previous observations, *PfA*-M17 crystallized as a functional hexamer, with two copies in the asymmetric unit; each structure of *PfA*-M17 therefore contains a total of 12 binding sites. Although minor differences in the quality of the ligand electron density are observed between the sites, the compound binding mode is largely conserved. Therefore, for clarity, when referring to structural features, we refer to the chain that showed the clearest electron density only (*PfA*-M17:7, chain B; *PfA*-M17:13l, chain C; *PfA*-M17:13m, chain C). The electron density was such that while racemic mixes of compounds were used for crystallization, only the *S*-enantiomer of **7** and the *R*-enantiomer of **13d**, **13l**, and **13m** could be modeled for both enzymes (Supplementary Figure 2, Supporting Information).

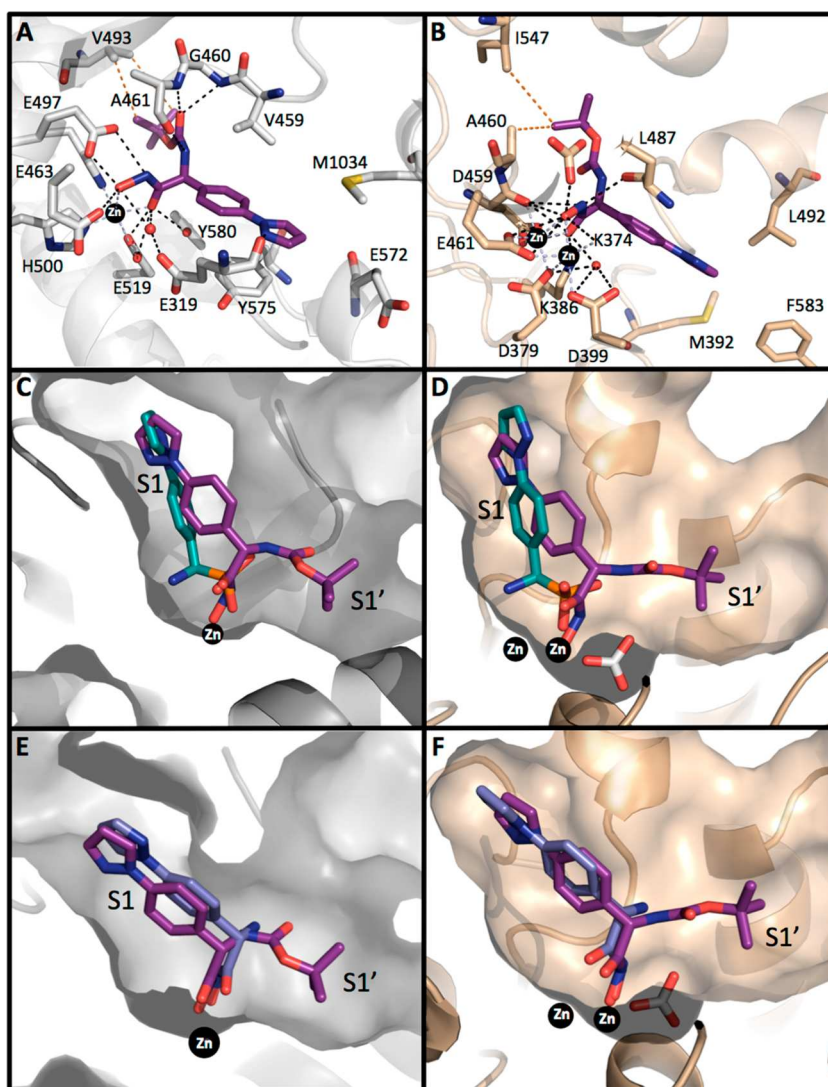


Figure 2. The hydroxamic acid scaffold allows compounds access to the S1' pocket of *PfA-M1* and *PfA-M17*. (A, B) Stick representation of the binding mode of compound 7 (purple) to (A) *PfA-M1* (gray) and (B) *PfA-M17* (beige). Hydrogen bonds are shown as black dashes, key hydrophobic interactions as orange dashes, zinc ions as black spheres, and ordered water molecules as orange spheres. (C, D) Overlay of the binding pose of **1**_{dock} (teal) and **7** (purple) in *PfA-M1* (C) and *PfA-M17* (D). The Boc group of **7** probes the S1' pocket of both enzymes. Active site zinc and carbonate ions are indicated. (E, F) Overlay of the binding pose of **7** (purple) and **8** (blue) in *PfA-M1* (E) and *PfA-M17* (F). The binding pose of compound **7** is dictated by the hydroxamic acid ZBG rather than the 4-(1*H*-pyrazol-1-yl)phenyl moiety.

The Geometry of the ZBG Dictates the Ligand Binding Position. The current series of compounds was anticipated to improve inhibitory potency by replacing the phosphonic acid ZBG present on **1**, a potent *PfA-M1*/*PfA-M17* inhibitor (Figure 1), with a hydroxamic acid moiety. As has been observed for all ligand-bound *PfA-M1* crystal structures to date, *PfA-M1*:**7** revealed the zinc ion to be coordinated by residues of the catalytic triad: His496, His500, and Glu519. In addition, both oxygen atoms of the hydroxamic acid moiety also coordinate the zinc ion. The hydroxamic acid moiety takes part in extensive hydrogen-bonding interactions with active site components: the OH with His500 and Glu497, the NH with Glu497 and an ordered water molecule (W1), and the carbonyl with Glu519, Tyr580, and W1 (Figure 2A). In total, the hydroxamic acid forms 12 metallo or hydrogen bonds with *PfA-M1*, in comparison to the 7 interactions made by the phosphonic acid of the parent compound **1**.

PfA-M17 has two catalytic zinc ions which are coordinated by Asp459, Lys374, Asp379, Asp399, and Glu461. The crystal

structure of *PfA-M17*:**7** shows the hydroxamic acid moiety coordinates both catalytic zinc ions, as well as forms hydrogen bonds to five active site residues: Leu487, Lys374, Asp379, Asp459, and Lys386. Additionally, the moiety forms a water-mediated hydrogen bond with Asp399 and interacts with the active site carbonate ion present in all *PfA-M17* structures (Figure 2B). Overall, the hydroxamic acid of **7** can make 14 potential interactions with *PfA-M17*, whereas the amino-phosphonic acid moiety present on **1** makes only 8. While the hydroxamic acid of **7** and phosphonic acid of **1** are bound in comparable positions in both *PfA-M1* and *PfA-M17*, the orientation of the 4-(1*H*-pyrazol-1-yl)phenyl system, which is common to both compounds, varies considerably (Figure 2C,D). In the active sites of both enzymes, the 4-(1*H*-pyrazol-1-yl)phenyl system of **7** is substantially translated and additionally rotated compared to that of **1**. This places the biaryl system of **7** in a different region of the pockets, stacking between Tyr575 and Val459 in *PfA-M1*:**7** and Phe398, Met396, and Gly489 in *PfA-M17*:**7**. While few other direct interactions

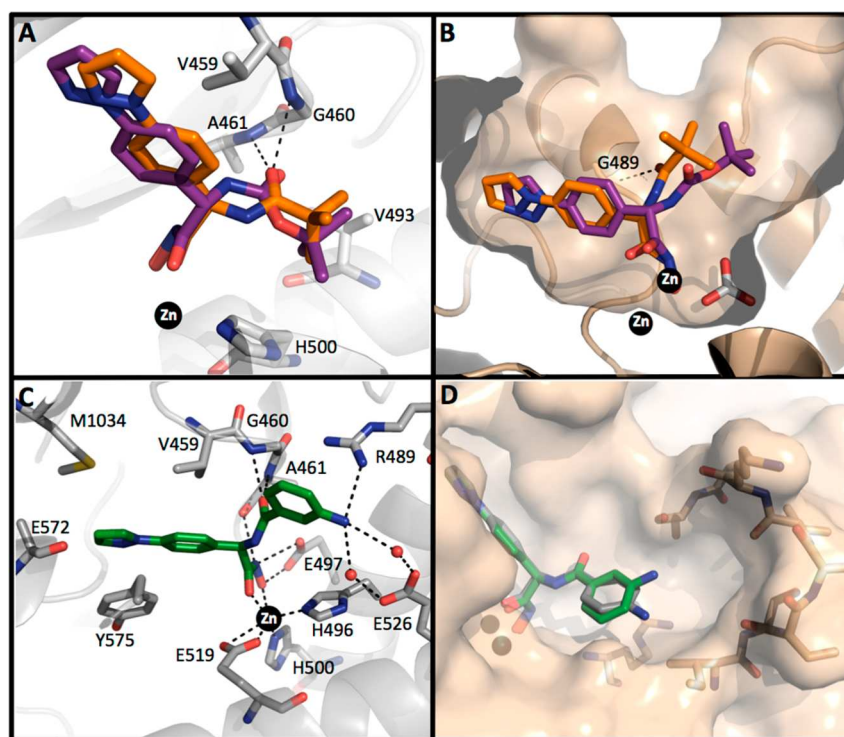


Figure 3. Structural investigation of the S1' pocket of *PfA-M1* and *PfA-M17*. (A) Overlay of the binding poses of **7** (purple) and **13d** (orange) to *PfA-M1* (gray). *PfA-M1* has an enantiomeric preference for (*S*)-**7** and (*R*)-**13d**, which allows the *tert*-butyl groups of both compounds to occupy similar space and interact with Val493. (B) Overlay of the binding poses of **7** (purple) and **13d_{dock}** (orange) to *PfA-M17* (beige). Similarly to *PfA-M1*, *PfA-M17* has an enantiomeric preference for (*S*)-**7** and (*R*)-**13d**; however, formation of a hydrogen bond between Gly489 (black dashes) directs the branched alkanes (*tert*-butyl in **13d**) out of the hydrophobic S1' cavity. (C) Binding mode of compound **13l** (green) to *PfA-M1*. Hydrogen bonds are shown as black dashes, the zinc ion is shown as a black sphere, and ordered water molecules are shown as red spheres. (D) Binding poses of **13l** (green) and **13m** (gray) in the *PfA-M17* cavity. The pocket is flanked by hydrophilic residues at the neck (shown in stick representation), and a small hydrophobic auxiliary cavity off the S1' pocket is visible.

are observed between the 4-(1*H*-pyrazol-1-yl)phenyl system and enzyme in either the *PfA-M1*:**7** or *PfA-M17*:**7** structure, the binding pose of **7** is more reminiscent of that observed for Bestatin than that of the parent aminophosphonic acid **1**. Bestatin is a Phe-Leu analogue inhibitor based on the transition state of the proteolysis reaction performed by *PfA-M1* and *PfA-M17*. When the Bestatin-bound *PfA-M1* (PDB ID 3EBH)⁷ and *PfA-M17* (PDB ID 3KR4)⁹ structures are overlaid with the corresponding structures bound to **7**, the benzyl group (Phe side chain) of Bestatin sits in the same position as the 4-(1*H*-pyrazol-1-yl)phenyl moiety and the *N*-Boc group of **7** occupies the same pocket as the Leu side chain of Bestatin (Supplementary Figure 3, Supporting Information). It is the altered binding position of **7** compared to that of **1** that allows the *N*-Boc group access to the S1' pocket. In *PfA-M1*:**1** and *PfA-M17*:**1**, the nitrogen atom of the 2-amino group points away from the S1' pocket and forms hydrogen bonds with Glu463 and Glu319 in *PfA-M1*:**1** and Asp399 in *PfA-M17*:**1**, whereas, in *PfA-M1*:**7** and *PfA-M17*:**7**, the corresponding nitrogen atom (now part of a carbamate group) is positioned to allow the *N*-Boc group to access the S1' pockets (Figure 2C,D). The altered binding pose conferred by the scaffold has different effects on *PfA-M1* and *PfA-M17* inhibitory activity. The aminophosphonic acid **1** and its structural analogue from the hydroxamic acid series, **8**, have similar *PfA-M1* inhibitory potencies ($K_i = 104$ and $74.5 \mu\text{M}$, respectively, Table 1), suggesting that the different binding pose does not come at any cost to binding. In contrast, direct exchange of the phosphonic acid for the hydroxamic acid ZBG has a detrimental effect on

the *PfA-M17* inhibitory activity; **1** has a K_i of $0.011 \mu\text{M}$ compared to $86 \mu\text{M}$ for **8**.

The change in binding pose of **1** versus **7** could result from the geometry of the different ZBGs and the nature of their interaction with the zinc ion(s) and/or steric limitations in the *PfA-M1* and *PfA-M17* S1 site for accommodation of the *N*-Boc group. To determine whether one or both of these factors promote the altered binding pose, we docked **8** into both enzymes (Supplementary Figures 4A and 5A, Supporting Information). In *PfA-M1*:**8_{dock}** the ligand has a binding pose similar to that of the ligand in **7** (Figure 2E), with the amine directed toward the S1' pocket and forming hydrogen bonds with the main chain nitrogen and oxygen atoms of Ala461. Thus, in *PfA-M1* it appears that the distinct interaction of the hydroxamic acid ZBG with the zinc ion may be responsible for the translated binding pose, relative to that of **1**. The structure of *PfA-M17*:**8_{dock}** positions the ligand further from the S1' pocket toward the S1 pocket (Figure 2F). This suggests that the *N*-Boc group present on **7** functions as an S1' anchor, and in its absence there may be some mobility of compound binding that contributes to the reduced affinity of this inhibitor. Regardless, similarly to *PfA-M1*:**8_{dock}** the binding pose of **8** in *PfA-M17*:**8_{dock}** is similar to that observed for **7**, again suggesting that it is the geometry of the ZBG that dictates the binding pose of **7**, not the *N*-Boc group. The altered binding pose observed upon substitution of the phosphonic acid for a hydroxamic acid suggests that exchange of a ZBG late in the lead optimization process may not be practical for the retention of other binding interactions in the active site. However, for this

compound series, the altered binding pose fortuitously offers the opportunity to exploit further interaction with the S1' pocket.

The Compound SARs for the S1' Pocket Are Different for Pfa-M1 versus Pfa-M17. The consequence of the altered binding pose brought about by substitution of the series' ZBG is that further functionalization of the free amine of **8** offers the potential to exploit binding interactions with the S1' pocket which were previously unavailable to this compound series. In both Pfa-M1:7 and Pfa-M17:7, the hydrophobic *N*-Boc group sits in the S1' pocket, in the position occupied by the side chain of Leu in Bestatin, forming favorable interactions with hydrophobic residues (Val493 in Pfa-M1; Ala460 and Ile547 in Pfa-M17) (Figure 2A,B). To probe the steric tolerance of these pockets, compounds with a range of aliphatic *N*-acyl groups (**13a–e**) as well as substituted *N*-benzoyl groups (**13f–i**) were tested for inhibitory activity at both Pfa-M1 and Pfa-M17; their capability to occupy the S1' pocket was examined using a combination of crystal and docked structures.

The *N*-acetyl derivative **13a** was found to have opposing effects on the inhibition of Pfa-M1 and Pfa-M17. While its Pfa-M1 inhibitory potency is roughly comparable to that of **8** ($K_i = 74.5 \mu\text{M}$; **13a**, $K_i = 113 \mu\text{M}$), it exhibited a considerable improvement in inhibitory potency for Pfa-M17 (**8**, $K_i = 86 \mu\text{M}$; **13a**, $K_i = 0.019 \mu\text{M}$) (Table 1). The docked structure of Pfa-M17:**13a** suggests that the additional carbonyl group is capable of picking up a hydrogen-bonding interaction with the backbone amine of Gly489 (Supplementary Figure 5, Supporting Information). This interaction is also observed in the structure of Bestatin bound to Pfa-M17, suggesting that it is also common to substrates of the enzyme and therefore is a good target in inhibitor design.

As the size and branching of the *N*-acyl group increase from acetyl (**13a**) to propionyl (**13b**), isovaleryl (**13c**), and pivaloyl (**13d**), a corresponding improvement in Pfa-M1 inhibitory potency is observed ($K_i = 113, 41.3, 12.3,$ and $0.7 \mu\text{M}$, respectively, Table 1). This indicates that increasing the steric bulk of the *N*-acyl substituent is favorable for binding to the Pfa-M1 S1' pocket. Docking analysis of each of these compounds indicates that their binding modes are highly conserved (Supplementary Figure 4, Supporting Information), suggesting that the additional space occupied by the larger substituents within the hydrophobic pocket contributes to improved binding. Compounds **13d** and **7**, the most potent Pfa-M1 inhibitors of the series, both bear *tert*-butyl moieties; however, **13d** bears an amide linker, compared to the corresponding carbamate linker present on **7**. The *tert*-butyl moiety of **13d** is therefore relatively closer to the ZBG. In the structure of Pfa-M1:7, the *tert*-butyl group sits deep within the S1' pocket and forms hydrophobic contacts with Val493 at the base. It was therefore not surprising that in the structure of Pfa-M1:**13d**_{dock} the shorter substituent of **13d** does not occupy the same space as the equivalent group in **7** and is unable to form hydrophobic interactions with Val493. However, given the lack of any additional interactions capable of compensating for this loss, it was curious that both **7** and **13d** demonstrated equivalent inhibitory potencies (K_i values of 0.8 and $0.7 \mu\text{M}$, respectively). We therefore determined the cocrystal structure of Pfa-M1 in complex with **13d** (Pfa-M1:**13d**). While a racemic mixture of the ligand was used for crystallization, only the *R*-enantiomer of **13d** was observed to bind Pfa-M1. This observation is in contrast to the Pfa-M1:7 structure, which showed only the *S*-enantiomer bound (Figure 3A). The switch

in enantiomeric preference allows the *tert*-butyl group of **13d** to occupy a space similar to that of the *tert*-butyl group of **7** and to maintain the hydrophobic interactions with Val493. This adjustment to maintain the interaction with Val493 emphasizes the importance of the interaction in the S1' pocket of Pfa-M1.

Catalytically, Pfa-M17 has a clear preference for bulky hydrophobic residues;⁴⁶ therefore, it was anticipated that compounds bearing increasingly hydrophobic *N*-acyl moieties would exhibit improved inhibitory potency. However, in contrast to the SAR observed with Pfa-M1, an increase in hydrophobic steric bulk from **13a** to **13d** showed very little effect on inhibition of Pfa-M17 (Table 1). When docked into the active site (Supplementary Figure 5, Supporting Information), it was observed that these compounds all form a hydrogen bond with Gly489 through the amide carbonyl oxygen atom. This hydrogen bond orientates short alkyl substituents out of the main hydrophobic S1' cavity (Figure 3B), explaining why additional steric presence in this region does not contribute to binding affinity.

The tolerance of the Pfa-M1 S1' pocket to a variety of substituted aromatic moieties was then examined with *N*-benzoyl-substituted (**13f**) and *N*-fluorobenzoyl-substituted (**13g–i**) derivatives. Docking analysis showed that the phenyl group of **13f** cannot be accommodated within interaction distance to Val493 and is instead directed to the solvent, accounting for the reduced Pfa-M1 inhibitory potency. Although the *N*-fluorobenzoyl-substituted compounds regained some of this potency, none inhibited Pfa-M1 as well as **7** or **13d**. However, beyond the hydrophobic edge of the S1' pocket of Pfa-M1, the region becomes increasingly solvated within the large C-terminal channel. This is the putative substrate entry channel, where both hydrophilic residues and ordered water molecules are observed. To take advantage of this dual nature of the pocket, *N*-aminobenzoyl-substituted derivatives **13l** and **13m** were also examined. Both compounds demonstrated moderate inhibitory activity (5.5 and $7.4 \mu\text{M}$, respectively, Table 1), and comparison of the crystal structure of Pfa-M1:**13l** and the docked structure of Pfa-M1:**13m**_{dock} showed that the amino substituent is placed in similar positions for both binding poses, where it is able to form a direct hydrogen bond with Arg489, in addition to water-mediated hydrogen bonds with Glu526 (Figure 3C). Elaboration of this moiety to take advantage of additional hydrogen-bonding partners may lead to an improved Pfa-M1 inhibitory potency of these compounds.

The same series of substituted *N*-benzoyl compounds (**13g–i** and **13l–m**) was tested for Pfa-M17 inhibitory activity and was found to effectively recover the loss of potency exhibited by **13f**. To determine the structural rationale for this difference, both **13l** and **13m** were cocrystallized with the enzyme. The two compounds bound with near-identical binding poses, with only the *R*-enantiomers of each observed. Similarly to **13a–d** at Pfa-M1, these enantiomers allow the *N*-acyl substituent to probe deeper into the S1' pocket. This region of the pocket contains more hydrophilic residues than the neck of the pocket, making it more favorable for the electronegative fluoro or polar amino substituents to occupy (Figure 3D). However, no direct interactions with the pocket were observed, and little variation was observed in compound inhibitory potencies. There does appear to be additional space in the Pfa-M17 S1' pocket, specifically a small auxiliary cavity, that is not occupied by **13l–m** (Figure 3D); further extension of this region of the scaffold to better fit the pocket may offer improvements in Pfa-M17 inhibition. Conversely, such extension is likely to be

detrimental to PfA-M1 inhibitor potency, as the PfA-M1 S1' pocket is less tolerant to aromatic moieties in this region.

The Hydroxamic Acid Compound Series Inhibits the Growth of *P. falciparum* 3D7. The described series of hydroxamic acid-based compounds contains the most potent dual PfA-M1/PfA-M17 inhibitors described to date. We therefore determined the ability of these compounds to inhibit the growth of the asexual erythrocytic stages of Pf-3D7 parasites, utilizing a well-established Pf imaging assay (Supplementary Figure 6, Supporting Information).⁴⁷ Briefly, the parasite number (and thus growth inhibition) was determined through measurement of the incorporation of the DNA-intercalating dye 4',6-diamidino-2-phenylindole into the parasite nucleus following exposure to the compounds. Fluorescent images acquired on PerkinElmer's Opera were analyzed with a spot detection algorithm using the Acapella software. Previous potent PfA-M1/PfA-M17 inhibitors Bestatin and CHR-6768 have been reported to demonstrate inhibitory potencies between 0.4 and 5 μM for Pf-3D7 parasite growth. Compounds from our present series inhibit parasite growth with IC_{50} values between 0.2 and 0.7 μM (Table 1), with the variation in potency in general agreement with changes in PfA-M1/PfA-M17 inhibitory activity. Compound **13d**, the most effective PfA-M1 inhibitor ($K_i = 0.7 \mu\text{M}$) and one of the more potent Pf-M17 inhibitors ($K_i = 0.028 \mu\text{M}$), is the most effective compound against 3D7 malaria parasites, with an IC_{50} of 227 nM (Table 1). Although the in vitro inhibitory properties of compound **7** are comparable to those of **13d**, it has an IC_{50} for parasite growth of only 783 nM, suggesting that compounds substituted with the *N*-Boc group are either less capable of cellular penetration or less stable than the corresponding *N*-acyl derivatives. Compounds **13l** and **13m** are also highly effective against the malaria parasites (IC_{50} values of 233 and 228 nM, respectively), despite slightly reduced affinity for Pf-M1 compared to **13d** (and comparable activity for Pf-M17). This could be attributed to indirect factors, such as improved cellular penetration or protozoan cytotoxicity arising from toxic metabolites produced by the parasite, which has the potential to be metabolically active during the 3D7 assay. We additionally screened all of the compounds in the series for cytotoxicity against human embryonic kidney cells (HEK293) and saw no observable cytotoxicity at concentrations up to 40 μM (Supplementary Figure 6). Although we have yet to perform stability and distribution studies, previous analyses of hydroxamic acid-based inhibitors suggest that the scaffold is capable of reaching the site of action within cultured erythrocytes,¹⁰ making this a promising scaffold for further development.

Hydroxamate-containing inhibitors of human aminopeptidase N have been identified,⁴⁸ and Bestatin has undergone clinical trials as an immunomodulating agent.^{49,50} Therefore, the potential for the compounds described here to act upon the human isoforms of PfA-M1 and/or PfA-M17 in vitro cannot be discounted. However, the lack of any observed toxicity of our compounds in HEK293 cells is encouraging for the continued development of the series. Homologous M1 and M17 aminopeptidases also function as key enzymes in other parasites^{51,52} and bacterial pathogens.^{53,54} This compound series may therefore have potential applications for the development of other MAP inhibitors for the treatment of a range of diseases.

CONCLUSIONS

The Pf aminopeptidases M1 and M17 are validated drug targets for antimalarial agents with a novel mode of action. While previous inhibitor series demonstrated that cross-inhibition was possible, differences in the compound binding profiles of the enzymes meant that compound elaboration tended toward improved inhibition of one enzyme target at the expense of the other. We report here the first series of compounds capable of potent dual inhibition of both PfA-M1 and PfA-M17. The series additionally possesses activity against 3D7 malaria parasites and no observable cytotoxicity. This hydroxamic acid-based series of compounds therefore provides extremely attractive lead molecules for further development into antimalarial compounds with a novel mode of action.

EXPERIMENTAL SECTION

Chemistry. Chemicals and solvents were purchased from standard suppliers and used without further purification. Davisil silica gel (40–63 μm), for flash column chromatography (FCC), was supplied by Grace Davison Discovery Sciences (Victoria, Australia), and deuterated solvents were purchased from Cambridge Isotope Laboratories, Inc. (United States, distributed by Novachem PTY. Ltd., Victoria, Australia).

Unless otherwise stated, reactions were carried out at ambient temperature. Reactions were monitored by thin-layer chromatography on commercially available precoated aluminum-backed plates (Merck Kieselgel 60 F₂₅₄). Visualization was by examination under UV light (254 and 366 nm). General staining was carried out with KMnO_4 or phosphomolybdic acid. A solution of ninhydrin (in ethanol) was used to visualize primary and secondary amines. A solution of FeCl_3 (5% in 0.5 M $\text{HCl}(\text{aq})$) was used to visualize hydroxamic acids. All organic extracts collected after aqueous workup procedures were dried over anhydrous Na_2SO_4 before gravity filtering and evaporation to dryness. Organic solvents were evaporated in vacuo at $\leq 40^\circ\text{C}$ (water bath temperature). Purification using preparative-layer chromatography (PLC) was carried out on Analtech preparative TLC plates (200 mm \times 200 mm \times 2 mm).

^1H NMR and ^{13}C NMR spectra were recorded on a Bruker Avance Nanobay III 400 MHz Ultrashield Plus spectrometer at 400.13 and 100.6 MHz, respectively. Chemical shifts (δ) are recorded in parts per million with reference to the chemical shift of the deuterated solvent. Coupling constants (J) and carbon–fluorine coupling constants (J_{CF}) are recorded in hertz and the significant multiplicities described as singlet (s), doublet (d), triplet (t), quadruplet (q), broad (br), multiplet (m), doublet of doublets (dd), and doublet of triplets (dt). Spectra were assigned using appropriate correlation spectroscopy (COSY), distortionless enhanced polarization transfer (DEPT), heteronuclear single-quantum correlation (HSQC), and heteronuclear multiple-bond correlation (HMBC) sequences.

LC/MS was run to verify the reaction outcome and purity using either system A or system B. System A: an Agilent 6100 series single-quadrupole instrument coupled to an Agilent 1200 series HPLC instrument. The following buffers were used: buffer A, 0.1% formic acid in H_2O ; buffer B, 0.1% formic acid in MeCN. The following gradient was used with a Phenomenex Luna 3 μM C8(2) 15 \times 4.6 mm column, a flow rate of 0.5 mL/min, and a total run time of 12 min: 0–4 min 95% buffer A and 5% buffer B, 4–7 min 0% buffer A and 100% buffer B, 7–12 min 95% buffer A and 5% buffer B. Mass spectra were acquired in positive and negative ion modes with a scan range of 0–1000 m/z at 5 V. UV detection was carried out at 254 nm. System B: an Agilent 6120 series single-quadrupole instrument coupled to an Agilent 1260 series HPLC instrument. The following buffers were used: buffer A, 0.1% formic acid in H_2O ; buffer B, 0.1% formic acid in MeCN. The following gradient was used with a Poroshell 120 EC-C18 50 \times 3.0 mm 2.7 μm column, a flow rate of 0.5 mL/min, and a total run time of 5 min: 0–1 min 95% buffer A and 5% buffer B, from 1 to 2.5 min up to 0% buffer A and 100% buffer B, held at this composition until 3.8 min, 3.8–4 min 95% buffer A and 5% buffer B, held until 5

min at this composition. Mass spectra were acquired in positive and negative ion modes with a scan range of 100–1000 m/z . UV detection was carried out at 214 and 254 nm. All retention times (t_R) are quoted in minutes.

Preparative HPLC was performed using an Agilent 1260 Infinity instrument coupled with a binary preparative pump and Agilent 1260 FC-PS fraction collector using Agilent OpenLAB CDS software (revision C.01.04) and an Altima 5 μ M C8 22 \times 250 mm column. The following buffers were used: buffer A, H₂O; buffer B, MeCN. The sample was run at a gradient of 5% buffer B to 100% buffer B over 20 min at a flow rate of 20 mL/min. All screening compounds were of >95% purity unless specified in the individual monologue.

General Procedure A: Condensation of Methyl 2-(4-(1H-Pyrazol-1-yl)phenyl)-2-aminoacetate Hydrochloride (11) with Acid Chlorides and Isocyanates. 11 (134 mg, 0.50 mmol) and TEA (0.154 mL, 1.10 mmol, 2.2 equiv in the case of acid chlorides, or 0.077 mL, 0.55 mmol, 1.1 equiv in the case of isocyanates) were dissolved in DCM (3 mL). To this was added the appropriate acid chloride (0.55 mmol, 1.1 equiv), and the mixture was stirred at room temperature for 18 h. Reaction progress was monitored by TLC (EtOAc/DCM, 1:1). On completion, the reaction mixtures were diluted with DCM (10 mL) and washed with water (10 mL). Concentration of the organic layer afforded the product, which was carried through to the next step with no further purification necessary.

General Procedure B: Direct Aminolysis of Methyl Esters to the Corresponding Hydroxamic Acids by Sequential Addition of Reagents. The appropriate methyl ester (0.40–0.55 mmol) and NH₂OH·HCl (139 mg, 2 mmol) were dispersed in MeOH (2 mL) at room temperature. To this was added in a dropwise fashion 5 M KOH/MeOH (0.5 mL, 2.5 mmol) further diluted in MeOH (to 10 mL). The mixtures were stirred at room temperature and monitored by LC/MS analysis. The mixtures were concentrated before acidification with either 1 M HCl(aq) (10 mL) or AcOH/water (1:1, 10 mL, for more acid sensitive compounds). The aqueous slurry was then extracted with EtOAc (3 \times 10 mL), and the combined organic layers were washed with brine (10 mL) and then dried of Na₂SO₄. Concentration of the organic layers gave the crude product, which was further purified by FCC (eluent MeOH/DCM, 0:100 to 10:90).

General Procedure C: Direct Aminolysis of Methyl Esters to the Corresponding Hydroxamic Acids with Premixing of Reagents Using Anhydrous MeOH. The appropriate methyl ester (0.40–0.55 mmol) was dissolved in anhydrous MeOH (0.5 mL) at room temperature in a nitrogen-flushed vessel. In a separate nitrogen-flushed vial, NH₂OH·HCl (139 mg, 2 mmol) and 5 M KOH/anhydrous MeOH (0.5 mL, 2.5 mmol) were mixed and then sonicated for 30 s. The resulting suspension was added to the methanolic ester solution with washings of anhydrous MeOH (1 mL). The mixtures were stirred at room temperature overnight and monitored by LC/MS analysis. The mixtures were directly dry-loaded onto Isolute HM-N (Biotage) before purification by FCC (eluent MeOH/DCM, 0:100 to 10:90).

General Procedure D: CDI-Mediated Coupling of Carboxylic Acids to Hydroxylamine To Give the Corresponding Hydroxamic Acid. The appropriate carboxylic acid (1 equiv) was dissolved in anhydrous THF (1–5 mL/mmol) at room temperature under an atmosphere of nitrogen, and CDI (1.5 equiv) was added. The mixture was stirred at room temperature for 1 h before addition of NH₂OH·HCl (2 equiv). Stirring was continued at room temperature for 24–48 h before dilution of the mixture with satd NH₄Cl(aq) (20 mL) and then extraction with EtOAc (3 \times 20 mL). The combined organic layers were washed with satd NaHCO₃(aq) (20 mL) and brine (20 mL) before concentration under reduced pressure. The resulting crude product was further purified by FCC (eluent MeOH/DCM, 0:100 to 10:90).

1-(4-(1H-Pyrazol-1-yl)phenyl)ethan-1-one (3).³¹ 4'-Iodoacetophenone (2) (16.15 g, 65.63 mmol), pyrazole (4.92 g, 72.19 mmol, 1.1 equiv), and Cs₂CO₃ (42.77 g, 131.26 mmol, 2.0 equiv) were placed in a dry flask under an atmosphere of nitrogen. To this was added dry DMF (100 mL). The solution was degassed by sonication before addition of Cu₂O (939 mg, 6.56 mmol, 0.1 equiv), and the resulting solution was heated at 100 °C for 17.5 h. The mixture was cooled

before being diluted with water (400 mL) and then extraction with EtOAc (4 \times 100 mL). The combined organic layers were washed with brine (100 mL) before being dried over MgSO₄, and then the organic solution was passed through a plug of silica gel. The filtrate was concentrated under reduced pressure and the resulting residue dissolved in DCM and passed through a second plug of silica gel, initially washing with DCM, followed by elution with EtOAc/DCM (1:1). On concentration of the filtrate, 11.8 g of pale blue solid was obtained (97%): ¹H NMR (CDCl₃) δ 8.10–8.04 (m, 2H), 8.01 (d, J = 2.5 Hz, 1H), 7.85–7.79 (m, 2H), 7.77 (d, J = 1.5 Hz, 1H), 6.52 (dd, J = 2.4/1.9 Hz, 1H), 2.62 (s, 3H); ¹³C NMR (CDCl₃) δ 197.0, 143.4, 142.2, 135.0, 130.1, 127.1, 118.5, 108.7, 26.7; MS (TOF ES⁺) m/z C₁₁H₁₁N₂O [MH]⁺ calcd 187.1, found 187.2; LC/MS t_R = 3.50.

2-(4-(1H-Pyrazol-1-yl)phenyl)-2-oxoacetic Acid (4). 3 (11.8 g, 63.37 mmol) and SeO₂ (9.6 g, 86.52 mmol, 1.37 equiv) were dispersed in anhydrous pyridine (300 mL) under an atmosphere of nitrogen gas and heated under reflux at 110 °C for 20 h. LC/MS analysis indicated almost complete conversion to the desired product, so SeO₂ (3.516 g, 31.69 mmol, 0.5 equiv) was added before heating was continued for a further 5 h. LC/MS analysis indicated the reaction was complete, so the reaction was cooled to room temperature with stirring overnight. The mixture was filtered and the filtrate concentrated under reduced pressure to remove pyridine. The resulting residue was taken up in 2 M HCl(aq) (200 mL) and extracted with EtOAc (300 mL, 2 \times 200 mL, 100 mL). The combined organic layers were then extracted with 2 M NaOH(aq) (2 \times 100 mL). The combined aqueous extracts were reacidified with concd HCl(aq) and reextracted with EtOAc (3 \times 200 mL). Finally, the combined organic layers were washed with brine (100 mL). The combined organic layers were concentrated until precipitation was observed. At this point, excess hexanes were added to the flask, and the resultant precipitate was collected by filtration (vacuum). After drying, 12.58 g (92%) of pale yellow solid was obtained: ¹H NMR (DMSO) δ 14.75 (s, 1H), 8.77–8.65 (m, 1H), 8.17–8.02 (m, 4H), 7.87 (d, J = 1.5 Hz, 1H), 6.65 (dd, J = 2.6/1.7 Hz, 1H); ¹³C NMR (DMSO) δ 184.3, 163.0, 141.1, 139.6, 128.5, 126.2, 125.7, 115.3, 106.2; MS (TOF ES⁺) m/z C₁₁H₉N₂O₃ [MH]⁺ calcd 217.1, found 217.1; LC/MS t_R = 2.67.

2-(4-(1H-Pyrazol-1-yl)phenyl)-2-((tert-butoxycarbonyl)amino)acetic Acid (5). 4 (500 mg, 2.31 mmol) was dispersed in dry 1,2-dichloroethane (20 mL) under an atmosphere of nitrogen. To this was added *N,N*-dibenzylamine (913 mg, 0.890 mL, 4.63 mmol, 2 equiv). The mixture was stirred at room temperature for 5 min before addition of Na(OAc)₃BH (980 mg, 4.63 mmol, 2 equiv). The mixture was then stirred at room temperature overnight. Workup of a small sample of reaction mixture in water/EtOAc and LC/MS analysis of each layer showed starting material and *N,N*-dibenzylamine partitioned into the aqueous layer, whereas the EtOAc layer contained product and some *N,N*-dibenzylamine. Further Na(OAc)₃BH (490 mg, 2.31 mmol, 1 equiv) was added and stirring continued at room temperature overnight. The mixture was diluted with water (50 mL) and stirred for 5 min before extraction with EtOAc (3 \times 50 mL). The combined organic layers were then washed with brine (50 mL), with the brine washings kept separate from the initial water layer. On washing with brine, precipitation of a white solid occurred. This was collected by filtration (vacuum) of both organic and brine layers and washing the collected solid with water. LC/MS analysis of this salt indicated it was the acetate salt of *N,N*-dibenzylamine. The organic layers were concentrated under reduced pressure and further purified by FCC (eluent MeOH/DCM, 0:100 to 5:95) to give 89 mg of *N*-(4-(1H-pyrazol-1-yl)benzyl)-*N*-benzyl-1-phenylmethanamine (decarboxylated product) and 702 mg of desired product contaminated with *N,N*-dibenzylamine.

The crude desired product was dissolved in MeOH/water (9:1, 20 mL) before addition of 10% Pd/C (70 mg). The mixture was hydrogenated (balloon) at room temperature overnight. LC/MS analysis indicated almost complete monodebenzylation, so water (15 mL) and concd HCl(aq) (1 mL) were added, along with further 10% Pd/C (70 mg) before continued hydrogenation was continued at room temperature for 3.5 h. LC/MS analysis after this time indicated complete *N*-benzyl deprotection to the primary amine had occurred.

The mixture was filtered through a bed of Celite (vacuum) with washings of MeOH before concentration under reduced pressure. The resulting crude residue was taken up in water (20 mL) and washed with Et₂O (20 mL) before being basified with satd NaHCO₃(aq). The aqueous layer was washed again with Et₂O (20 mL) and the organic layer discarded. Boc₂O (555 mg, 2.54 mmol) was added to the aqueous layer and the mixture stirred at room temperature for 30 min before addition of further Boc₂O (252 mg, 1.15 mmol) and THF (10 mL). The mixture was stirred at room temperature overnight. After this time the mixture was carefully acidified to pH 4 with 2 M HCl(aq) before extraction with DCM (3 × 50 mL). The combined organic layers were concentrated under reduced pressure before further purification with FCC (eluent MeOH/DCM, 0:100 to 10:90) to give 410 mg of foamy white solid (56% over three steps): ¹H NMR (DMSO) δ 12.86 (s, 1H), 8.49 (d, *J* = 2.4 Hz, 1H), 7.81 (d, *J* = 8.5 Hz, 2H), 7.74 (d, *J* = 1.5 Hz, 1H), 7.66 (d, *J* = 8.3 Hz, 1H), 7.51 (d, *J* = 8.6 Hz, 2H), 6.54 (dd, *J* = 2.3/1.9 Hz, 1H), 5.15 (d, *J* = 8.2 Hz, 1H), 1.39 (s, 9H); ¹³C NMR (DMSO) δ 172.2, 155.2, 141.1, 139.2, 135.3, 128.9, 127.8, 118.3, 107.9, 78.5, 57.1, 28.2; MS (TOF ES⁺) *m/z* C₁₆H₂₀N₃O₄ [MH]⁺ calcd 318.1, found 318.2; LC/MS *t_R* = 3.18.

2-(4-(1H-Pyrazol-1-yl)phenyl)-2-aminoacetic Acid Hydrochloride (6). **5** (38 mg, 0.12 mmol) was dissolved in DCM (3 mL) before addition of 4 M HCl/1,4-dioxane (1 mL). The mixture was stirred at room temperature for 1 h before concentration under reduced pressure to give 29 mg of white solid (97%): ¹H NMR (DMSO) δ 13.96 (s, 1H), 8.91 (s, 3H), 8.55 (d, *J* = 2.4 Hz, 1H), 7.94 (d, *J* = 8.7 Hz, 2H), 7.78 (d, *J* = 1.5 Hz, 1H), 7.63 (d, *J* = 8.7 Hz, 2H), 6.58 (dd, *J* = 2.4/1.8 Hz, 1H), 5.18 (s, 1H); ¹³C NMR (DMSO) δ 169.7, 141.4, 140.2, 130.9, 129.5, 128.0, 118.6, 108.3, 54.9; MS (TOF ES⁺) *m/z* C₁₁H₁₂N₃O₂ [MH]⁺ calcd 218.1, found 218.1; LC/MS *t_R* = 1.39.

tert-Butyl (1-(4-(1H-Pyrazol-1-yl)phenyl)-2-(hydroxyamino)-2-oxoethyl)carbamate (7). **5** (100 mg, 0.32 mmol) was dissolved in dry THF (1 mL) under an atmosphere of nitrogen at room temperature. To this was added CDI (76 mg, 0.47 mmol, 1.5 equiv) and the mixture was stirred for 1 h at room temperature. Hydroxylamine hydrochloride (44 mg, 0.63 mmol, 2 equiv) was added, and the mixture was then stirred at room temperature overnight. LC/MS analysis indicated approximately 75% conversion had taken place, so stirring was continued for a further 3 days. Satd NH₄Cl(aq) (20 mL) was added before extraction with EtOAc (3 × 20 mL). The combined organic layers were then washed with brine (20 mL). After concentration of the organic layers, the crude residue was further purified by PLC (NH₄OH/MeOH/DCM, 1:10:89), with the plate being run twice, to give 73 mg of white solid (69%): ¹H NMR (DMSO) δ 10.91 (s, 1H), 9.00 (s, 1H), 8.48 (d, *J* = 2.4 Hz, 1H), 7.79 (d, *J* = 8.7 Hz, 2H), 7.73 (d, *J* = 1.4 Hz, 1H), 7.58–7.45 (m, 3H), 6.54 (dd, *J* = 2.4/1.8 Hz, 1H), 5.08 (d, *J* = 8.6 Hz, 1H), 1.38 (s, 9H); ¹³C NMR (DMSO) δ 171.7, 166.9, 141.0, 139.1, 134.2, 128.3, 127.8, 118.2, 107.9, 80.5, 54.9, 28.2; MS (TOF ES⁻) *m/z* C₁₆H₁₉N₄O₄ [M - H]⁻ calcd 331.1, found 331.2; LC/MS *t_R* = 3.02.

2-(4-(1H-Pyrazol-1-yl)phenyl)-2-amino-N-hydroxyacetamide Hydrochloride (8). **7** (62 mg, 0.19 mmol) was dissolved in MeOH/DCM (1:1, 4 mL). To this was added 4 M HCl/1,4-dioxane (2 mL), and the mixture was stirred at room temperature for 2 h. The mixture was concentrated under reduced pressure to give 47 mg of hygroscopic yellow solid. This was further purified by preparative HPLC to give 13 mg of colorless semisolid (25%): ¹H NMR (MeOD) δ 8.29 (d, *J* = 2.5 Hz, 1H), 7.87 (d, *J* = 8.6 Hz, 2H), 7.75 (d, *J* = 1.5 Hz, 1H), 7.64 (d, *J* = 8.6 Hz, 2H), 6.56 (dd, *J* = 2.4/1.9 Hz, 1H), 4.86 (s, 1H); ¹³C NMR (MeOD) δ 167.0, 142.7, 142.3, 133.5, 130.3, 129.1, 120.7, 109.3, 55.6; MS (TOF ES⁺) *m/z* C₁₁H₁₃N₄O₂ [MH]⁺ calcd 233.1, found 233.1; LC/MS *t_R* = 1.49.

2-(4-(1H-Pyrazol-1-yl)phenyl)-2-(benzylamino)acetic Acid (9). **4** (6.00 g, 27.75 mmol) was dispersed in anhydrous 1,2-dichloroethane (240 mL) under an atmosphere of nitrogen at room temperature. To this stirred suspension was added benzylamine (5.95 g, 6.06 mL, 55.51 mmol, 2 equiv), and stirring was continued at room temperature for 5 min. Na(OAc)₃BH (11.77 g, 55.51 mmol, 2 equiv) was added in portions, and stirring was continued at room temperature overnight. The mixture was concentrated and the resulting residue partitioned

between water (200 mL) and EtOAc (100 mL) and stirred for 30 min at room temperature. The organic solvent was then removed under reduced pressure and the resulting solid collected by filtration (vacuum) and washed with water. After drying, 6.45 g (76%) of off-white solid was obtained, which was used without further purification. ¹H NMR analysis proved difficult due to poor solubility in a variety of solvents, including DMSO, and the obtained spectra were difficult to interpret due to peak broadness. LC/MS analysis gave a single peak with the correct mass, so NMR analysis was carried out in the subsequent step to confirm the structure: MS (TOF ES⁺) *m/z* C₁₈H₁₈N₃O₂ [MH]⁺ calcd 308.1, found 308.2; LC/MS *t_R* = 3.13.

Methyl 2-(4-(1H-Pyrazol-1-yl)phenyl)-2-(benzylamino)acetate (10). **9** (6.34 g, 20.61 mmol) was dispersed in MeOH (200 mL). To this was added concd H₂SO₄(aq) (2 mL), and the resulting mixture was boiled under reflux for 24 h before addition of further concd H₂SO₄(aq) (1 mL). Heating was continued for a further 24 h period. LC/MS analysis indicated the reaction was progressing slowly, so MeOH (100 mL) was added and heating continued for a further 72 h. LC/MS analysis indicated the reaction was complete, so the mixture was cooled before being concentrated under reduced pressure. The resulting residue was basified with satd NaHCO₃(aq) (250 mL) before extraction with DCM (3 × 100 mL). The combined organic layers were concentrated under reduced pressure and the resulting residue purified by FCC (eluent EtOAc/PE, 0:100 to 30:70, with a plateau at 15:85) to give 5.90 g (89%) of pale yellow oil: ¹H NMR (CDCl₃) δ 7.96–7.90 (m, 1H), 7.90–7.70 (m, 3H), 7.69–7.53 (m, 2H), 7.49–7.28 (m, 5H), 6.54–6.40 (m, 1H), 4.70–4.45 (m, 1H), 4.44–4.02 (m, 1H), 3.95–3.75 (m, 2H), 3.75–3.64 (m, 2H); ¹³C NMR (CDCl₃) δ 172.2, 141.7, 140.0, 139.9, 138.1, 130.1, 129.53, 129.4, 129.0, 128.5, 126.9, 119.7, 108.2, 63.6, 53.2, 52.7; MS (TOF ES⁺) *m/z* C₁₉H₂₀N₃O₂ [MH]⁺ calcd 322.2, found 322.2; LC/MS *t_R* = 3.21. ¹H/¹³C NMR spectra indicate multiple conformational states.

Methyl 2-(4-(1H-Pyrazol-1-yl)phenyl)-2-aminoacetate Hydrochloride (11). **10** (6.047 g, 18.82 mmol) was dissolved in MeOH (250 mL) and concd (32%) HCl(aq) (4 mL) before addition of 10% Pd/C (600 mg, 0.1 equiv by weight). The mixture was hydrogenated (balloon) at room temperature for 48 h. LC/MS analysis indicated complete conversion had taken place. The mixture was filtered through a bed of Celite with washings of MeOH. The filtrate was concentrated under reduced pressure and the resulting residue dispersed in satd NaHCO₃(aq) before extraction with DCM (3 × 100 mL). The combined organic layers were concentrated under reduced pressure to give 5.507 g of crude product. This was taken up in Et₂O/DCM before addition of a solution of 1 M HCl/Et₂O (25 mL). The resulting solution was stirred at room temperature for 30 min before being diluted with Et₂O, and the resulting precipitate was filtered to give 4.407 g (87%) of white amorphous solid: ¹H NMR (DMSO) δ 9.13 (d, *J* = 3.3 Hz, 3H), 8.56 (d, *J* = 2.3 Hz, 1H), 7.94 (d, *J* = 8.7 Hz, 2H), 7.78 (d, *J* = 1.5 Hz, 1H), 7.63 (d, *J* = 8.7 Hz, 2H), 6.58 (dd, *J* = 2.4/1.8 Hz, 1H), 5.36 (q, *J* = 5.0 Hz, 1H), 3.73 (s, 3H); ¹³C NMR (DMSO) δ 168.8, 141.5, 140.4, 130.1, 129.7, 128.0, 118.6, 108.3, 54.7, 53.3; MS (TOF ES⁺) *m/z* C₁₂H₁₄N₃O₂ [MH]⁺ calcd 232.1, found 232.2; LC/MS *t_R* = 3.02.

Methyl 2-(4-(1H-Pyrazol-1-yl)phenyl)-2-acetamidoacetate (12a). Acetyl chloride (0.039 mL, 0.55 mmol, 1.1 equiv) was reacted as described in general procedure A. After 24 h, further acetyl chloride (0.4 equiv) and triethylamine (0.5 equiv) were added, and stirring was continued for 24 h prior to workup to give 128 mg (93%) of off-white solid: ¹H NMR (CDCl₃) δ 7.91 (d, *J* = 2.4 Hz, 1H), 7.73 (d, *J* = 1.5 Hz, 1H), 7.72–7.65 (m, 2H), 7.51–7.41 (m, 2H), 6.57 (d, *J* = 6.7 Hz, 1H), 6.48 (dd, *J* = 2.4, 1.9 Hz, 1H), 5.62 (d, *J* = 7.1 Hz, 1H), 3.75 (s, 3H), 2.31 (s, 1H), 2.06 (s, 3H); ¹³C NMR (CDCl₃) δ 171.4, 169.5, 141.4, 140.3, 135.0, 128.6, 127.0, 119.8, 108.0, 56.0, 53.1, 23.2; MS (TOF ES⁺) *m/z* C₁₄H₁₆N₃O₃ [MH]⁺ calcd 274.1, found 274.1; LC/MS *t_R* = 3.30.

Methyl 2-(4-(1H-Pyrazol-1-yl)phenyl)-2-propionamidoacetate (12b). Propionyl chloride (0.048 mL, 0.55 mmol, 1.1 equiv) was reacted as described in general procedure A to give 135 mg (93%) of pale pink solid: ¹H NMR (CDCl₃) δ 7.95–7.89 (m, 1H), 7.75 (d, *J* = 1.5 Hz, 1H), 7.73–7.66 (m, 2H), 7.50–7.42 (m, 2H), 6.52 (d, *J* = 6.7

H₂, 1H), 6.48 (dd, *J* = 2.4, 1.9 Hz, 1H), 5.62 (d, *J* = 7.0 Hz, 1H), 3.75 (s, 3H), 2.30 (dd, *J* = 7.6/3.1 Hz, 2H), 2.23 (s, 1H), 1.17 (t, *J* = 7.6 Hz, 3H); ¹³C NMR (CDCl₃) δ 173.2, 171.5, 141.3, 140.2, 135.2, 128.6, 127.1, 119.8, 108.0, 55.9, 53.1, 29.5, 9.6; MS (TOF ES⁺) *m/z* C₁₅H₁₈N₃O₃ [MH]⁺ calcd 288.1, found 288.2; LC/MS *t_R* = 3.40.

Methyl 2-(4-(1H-Pyrazol-1-yl)phenyl)-2-isobutyramidoacetate (12c). Isobutyryl chloride (0.058 mL, 0.55 mmol, 1.1 equiv) was reacted as described in general procedure A to give 129 mg (85%) of off-white solid: ¹H NMR (CDCl₃) δ 7.95–7.90 (m, 1H), 7.74 (d, *J* = 1.7 Hz, 1H), 7.73–7.66 (m, 2H), 7.50–7.41 (m, 2H), 6.54 (d, *J* = 6.7 Hz, 1H), 6.48 (dd, *J* = 2.4/1.9 Hz, 1H), 5.60 (d, *J* = 6.9 Hz, 1H), 3.75 (s, 3H), 2.46 (hept, *J* = 6.9 Hz, 1H), 2.33 (s, 1H), 1.19 (d, *J* = 6.8 Hz, 3H), 1.15 (d, *J* = 6.9 Hz, 3H); ¹³C NMR (CDCl₃) δ 176.4, 171.5, 141.4, 140.2, 135.2, 128.5, 127.0, 119.8, 108.0, 55.8, 53.1, 35.5, 31.1, 19.6, 19.5; MS (TOF ES⁺) *m/z* C₁₆H₂₀N₃O₃ [MH]⁺ calcd 302.1, found 302.2; LC/MS *t_R* = 3.49.

Methyl 2-(4-(1H-Pyrazol-1-yl)phenyl)-2-pivalamidoacetate (12d). Pivaloyl chloride (0.068 mL, 0.55 mmol, 1.1 equiv) was reacted as described in general procedure A to give 152 mg (96%) of off-white solid: ¹H NMR (CDCl₃) δ 7.92 (d, *J* = 2.4 Hz, 1H), 7.76 (d, *J* = 1.6 Hz, 1H), 7.70 (d, *J* = 8.6 Hz, 2H), 7.45 (d, *J* = 8.5 Hz, 2H), 6.72 (d, *J* = 6.3 Hz, 1H), 6.56–6.40 (m, 1H), 5.56 (d, *J* = 6.6 Hz, 1H), 3.75 (s, 3H), 2.24 (s, 1H), 1.23 (s, 9H); ¹³C NMR (CDCl₃) δ 178.0, 171.6, 141.3, 140.2, 135.3, 128.5, 127.0, 119.9, 108.0, 56.0, 53.1, 38.8, 27.5; MS (TOF ES⁺) *m/z* C₁₇H₂₂N₃O₃ [MH]⁺ calcd 316.2, found 316.2; LC/MS *t_R* = 3.63.

Methyl 2-(4-(1H-Pyrazol-1-yl)phenyl)-2-(3-tert-butylureido)acetate (12e). *tert*-Butyl isocyanate (0.063 mL, 0.55 mmol, 1.1 equiv) was reacted as described in general procedure A to give 150 mg (91%) of off-white foamy solid: ¹H NMR (CDCl₃) δ 7.94–7.89 (m, 1H), 7.73 (d, *J* = 1.5 Hz, 1H), 7.70–7.64 (m, 2H), 7.49–7.41 (m, 2H), 6.47 (dd, *J* = 2.4/1.9 Hz, 1H), 5.49 (s, 1H), 3.73 (s, 3H), 3.39 (s, 2H), 1.32 (s, 9H); ¹³C NMR (CDCl₃) δ 172.1, 156.3, 141.1, 139.9, 135.9, 128.5, 127.3, 119.9, 108.1, 77.5, 77.4, 77.2, 76.8, 56.7, 53.1, 51.2, 29.5; MS (TOF ES⁺) *m/z* C₁₇H₂₃N₄O₃ [MH]⁺ calcd 331.2, found 331.2; LC/MS *t_R* = 3.57.

Methyl 2-(4-(1H-Pyrazol-1-yl)phenyl)-2-benzamidoacetate (12f). Benzoyl chloride (0.064 mL, 0.55 mmol, 1.1 equiv) was reacted as described in general procedure A to give 166 mg (99%) of off-white solid: ¹H NMR (CDCl₃) δ 7.92 (d, *J* = 2.2 Hz, 1H), 7.87–7.80 (m, 2H), 7.75 (d, *J* = 1.5 Hz, 1H), 7.74–7.69 (m, 2H), 7.59–7.50 (m, 3H), 7.49–7.41 (m, 2H), 6.49 (dd, *J* = 2.4/1.9 Hz, 1H), 5.81 (d, *J* = 6.7 Hz, 1H), 3.79 (s, 3H), 2.34 (s, 1H); ¹³C NMR (CDCl₃) δ 171.4, 166.7, 141.2, 140.1, 135.2, 133.6, 132.2, 128.8, 128.7, 127.3, 127.2, 119.9, 108.1, 56.4, 53.3; MS (TOF ES⁺) *m/z* C₁₉H₁₈N₃O₃ [MH]⁺ calcd 336.1, found 336.1; LC/MS *t_R* = 3.62.

Methyl 2-(4-(1H-Pyrazol-1-yl)phenyl)-2-(2-fluorobenzamido)acetate (12g). 2-Fluorobenzoyl chloride (0.066 mL, 0.55 mmol, 1.1 equiv) was reacted as described in general procedure A. The reaction was complete within 90 min and, after workup, gave 186 mg of off-white solid (quantitative): ¹H NMR (CDCl₃) δ 8.07 (ddd, *J* = 7.9/7.9/1.8 Hz, 1H), 7.92 (dd, *J* = 2.5/0.5 Hz, 1H), 7.89 (dd, *J* = 6.9/6.3 Hz, 1H), 7.75 (d, *J* = 1.5 Hz, 1H), 7.74–7.69 (m, 2H), 7.60–7.54 (m, 2H), 7.50 (dddd, *J* = 8.3/7.3/5.2/1.9 Hz, 1H), 7.28–7.23 (m, 1H), 7.16 (ddd, *J* = 12.1/8.3/0.9 Hz, 1H), 6.49 (dd, *J* = 2.4/1.9 Hz, 1H), 5.81 (dd, *J* = 6.4/1.8 Hz, 1H), 3.79 (s, 3H), 2.09 (s, 1H); ¹⁹F NMR (376 MHz, CDCl₃) δ –112.78; ¹³C NMR (CDCl₃) δ 171.1, 167.0, 161.1 (d, *J_{CF}* = 248.2 Hz), 141.4, 140.4, 134.8, 134.0 (d, *J_{CF}* = 9.4 Hz), 132.2 (d, *J_{CF}* = 1.9 Hz), 128.7, 126.9, 125.0 (d, *J_{CF}* = 3.2 Hz), 124.8, 119.8, 116.3 (d, *J_{CF}* = 24.7 Hz), 108.0, 56.8, 53.2; MS (TOF ES⁺) *m/z* C₁₉H₁₇FN₃O₃ [MH]⁺ calcd 354.1, found 354.2; LC/MS *t_R* = 3.68.

Methyl 2-(4-(1H-Pyrazol-1-yl)phenyl)-2-(3-fluorobenzamido)acetate (12h). 3-Fluorobenzoic acid (74 mg, 0.53 mmol, 1.05 equiv) and HCTU (228 mg, 0.55 mmol, 1.1 equiv) were dissolved in DMF (0.5 mL) at room temperature. DIPEA (0.193 mL, 1.10 mmol, 2.2 equiv) was added, followed by **11** (134 mg, 0.50 mmol) and DCM (0.5 mL). The mixture was stirred at room temperature for 135 min before LC/MS analysis indicated complete conversion had taken place. Satd NaHCO₃(aq)/water (1:1) (20 mL) was added and the aqueous slurry extracted with Et₂O (3 × 10 mL). The combined

organic layers were washed with brine (10 mL) before being concentrated under reduced pressure to give 189 mg (100%) of pale brown solid, which was used without further purification: ¹H NMR (CDCl₃) δ 7.92 (d, *J* = 2.2 Hz, 1H), 7.74 (d, *J* = 1.5 Hz, 1H), 7.73–7.69 (m, 2H), 7.65–7.50 (m, 4H), 7.43 (ddd, *J* = 8.0/8.0/5.5 Hz, 1H), 7.23 (dddd, *J* = 8.3/8.3/2.6/1.0 Hz, 2H), 6.48 (dd, *J* = 2.4/1.9 Hz, 1H), 5.78 (d, *J* = 6.7 Hz, 1H), 3.80 (s, 3H), 2.20 (s, 1H); ¹⁹F NMR (376 MHz, CDCl₃) δ –111.49; ¹³C NMR (CDCl₃) δ 171.2, 164.2, 164.0 (d, *J_{CF}* = 279.3 Hz), 141.1, 140.0, 135.9, 135.1, 130.5 (d, *J_{CF}* = 7.9 Hz), 128.7, 127.3, 122.7 (d, *J_{CF}* = 3.1 Hz), 120.0, 119.2 (d, *J_{CF}* = 21.2 Hz), 114.8 (d, *J_{CF}* = 23.0 Hz), 108.1, 56.5, 53.4; MS (TOF ES⁺) *m/z* C₁₉H₁₇FN₃O₃ [MH]⁺ calcd 354.1, found 354.2; LC/MS *t_R* = 3.66.

Methyl 2-(4-(1H-Pyrazol-1-yl)phenyl)-2-(4-fluorobenzamido)acetate (12i). 4-Fluorobenzoic acid (74 mg, 0.53 mmol, 1.05 equiv) was coupled to **11** (134 mg, 0.50 mmol) according to the procedure described for the synthesis of **12h** to give 214 mg (100%) of pale brown solid, which was used without further purification: ¹H NMR (CDCl₃) δ 7.94–7.91 (m, 1H), 7.88–7.81 (m, 2H), 7.74 (d, *J* = 1.7 Hz, 1H), 7.73–7.68 (m, 2H), 7.57–7.51 (m, 2H), 7.16–7.09 (m, 2H), 6.58–6.33 (m, 1H), 5.78 (d, *J* = 6.7 Hz, 1H), 3.79 (s, 3H), 2.27 (s, 1H); ¹⁹F NMR (376 MHz, CDCl₃) δ –107.24; ¹³C NMR (CDCl₃) δ 171.4, 165.6, 165.3 (d, *J_{CF}* = 284.8 Hz), 141.4, 138.9, 135.0, 131.9, 129.7 (d, *J_{CF}* = 9.0 Hz), 128.7, 127.0, 119.9, 115.9 (d, *J_{CF}* = 22.0 Hz), 108.1, 56.5, 53.3; MS (TOF ES⁺) *m/z* C₁₉H₁₇FN₃O₃ [MH]⁺ calcd 354.1, found 354.2; LC/MS *t_R* = 3.64.

Methyl 2-(4-(1H-Pyrazol-1-yl)phenyl)-2-(3-nitrobenzamido)acetate (12j). 3-Nitrobenzoyl chloride (102 mg, 0.55 mmol, 1.1 equiv) was reacted as described in general procedure A. After 4 h, further 3-nitrobenzoyl chloride (27 mg, 0.3 equiv) and TEA (0.035 mL, 0.5 equiv) were added, and stirring was continued for 24 h. LC/MS analysis indicated incomplete conversion, so 3-nitrobenzoyl chloride (46 mg, 0.5 equiv) and TEA (0.035 mL, 0.5 equiv) were added again, and stirring was continued for a further 24 h prior to workup to give 188 mg (99%) of pink solid: ¹H NMR (CDCl₃) δ 8.66 (dd, *J* = 1.9/1.9 Hz, 1H), 8.39 (ddd, *J* = 8.2/2.2/1.0 Hz, 1H), 8.22–8.15 (m, 1H), 7.93 (dd, *J* = 2.5/0.4 Hz, 1H), 7.77–7.71 (m, 3H), 7.67 (dd, *J* = 7.9/7.9 Hz, 1H), 7.58–7.51 (m, 2H), 7.37 (d, *J* = 6.0 Hz, 1H), 6.49 (dd, *J* = 2.4/1.9 Hz, 1H), 5.80 (d, *J* = 6.7 Hz, 1H), 3.81 (s, 3H); ¹³C NMR (CDCl₃) δ 171.1, 164.3, 148.4, 141.3, 140.2, 135.2, 134.6, 133.3, 130.1, 128.8, 127.2, 126.7, 122.3, 120.0, 108.2, 77.5, 77.4, 77.2, 76.8, 56.7, 53.5; MS (TOF ES⁺) *m/z* C₁₉H₁₇N₄O₅ [MH]⁺ calcd 381.1, found 381.2; LC/MS *t_R* = 3.66.

Methyl 2-(4-(1H-Pyrazol-1-yl)phenyl)-2-(4-nitrobenzamido)acetate (12k). 4-Nitrobenzoyl chloride (102 mg, 0.55 mmol, 1.1 equiv) was reacted as described in general procedure A. After 4 h, additional 4-nitrobenzoyl chloride (27 mg, 0.3 equiv) and TEA (0.035 mL, 0.5 equiv) were added, and stirring was continued for 24 h prior to workup. In this case, the mixture was diluted with EtOAc (20 mL) and then washed with water (10 mL) and satd NaHCO₃(aq) (10 mL). The organic layers were concentrated under reduced pressure to give 162 mg (85%) of pink solid: ¹H NMR (CDCl₃) δ 8.36–8.28 (m, 2H), 8.05–7.96 (m, 2H), 7.93 (d, *J* = 2.4 Hz, 1H), 7.78 (d, *J* = 1.7 Hz, 1H), 7.74 (d, *J* = 8.6 Hz, 2H), 7.55 (d, *J* = 8.5 Hz, 2H), 6.56–6.46 (m, 1H), 5.79 (d, *J* = 6.6 Hz, 1H), 3.81 (s, 3H); ¹³C NMR (CDCl₃) δ 171.2, 165.6, 150.0, 141.5, 139.1, 137.4, 135.0, 128.7, 128.6, 127.0, 124.1, 119.9, 108.2, 56.7, 53.5; MS (TOF ES⁺) *m/z* C₁₉H₁₇N₄O₅ [MH]⁺ calcd 381.1, found 381.2; LC/MS *t_R* = 3.65.

Methyl 2-(4-(1H-Pyrazol-1-yl)phenyl)-2-(3-aminobenzamido)acetate (12l). **12j** (115 mg, 0.30 mmol) was dispersed in MeOH (20 mL) and 10% Pd/C (10 mg) added under an atmosphere of nitrogen. The reaction flask was sealed before evacuation and replacement of the atmosphere with hydrogen. The mixture was then stirred under an atmosphere of hydrogen (balloon) for 1 h at room temperature. LC/MS analysis after this time indicated that complete conversion had taken place, so the mixture was filtered through a bed of Celite with washings of MeOH. The filtrate was concentrated under reduced pressure to give 102 mg (97%) of off-white glassy solid, which was used without further purification: ¹H NMR (CDCl₃) δ 7.89 (d, *J* = 1.8 Hz, 1H), 7.70 (s, 1H), 7.66 (d, *J* = 8.4 Hz, 2H), 7.49 (d, *J* = 8.3 Hz, 2H), 7.42–7.30 (m, 1H), 7.23–7.04

(m, 3H), 6.81 (s, 1H), 6.44 (s, 1H), 5.76 (d, $J = 6.8$ Hz, 1H), 4.16–3.53 (m, 5H); ^{13}C NMR (CDCl_3) δ 171.4, 167.1, 147.0, 141.4, 140.3, 134.8, 134.6, 129.6, 128.6, 126.9, 119.6, 118.5, 116.7, 113.9, 107.9, 56.4, 53.1; MS (TOF ES^+) m/z $\text{C}_{19}\text{H}_{19}\text{N}_4\text{O}_3$ $[\text{MH}]^+$ calcd 351.1, found 351.2; LC/MS $t_{\text{R}} = 3.37$.

Methyl 2-(4-(1H-Pyrazol-1-yl)phenyl)-2-(4-aminobenzamido)acetate (12m). 12k (62 mg, 0.16 mmol) was hydrogenated according to the procedure described for the synthesis of 12l to give 51 mg (91%) of brown solid: ^1H NMR (CDCl_3) δ 8.85–7.06 (m, 11H), 6.97–6.21 (m, 3H), 5.82 (s, 1H), 3.85 (s, 3H); ^{13}C NMR (CDCl_3) δ 171.6, 166.5, 150.3, 141.4, 140.2, 135.1, 129.1, 128.6, 126.9, 122.7, 119.6, 114.2, 107.9, 56.3, 53.1; MS (TOF ES^+) m/z $\text{C}_{19}\text{H}_{19}\text{N}_4\text{O}_3$ $[\text{MH}]^+$ calcd 351.1, found 351.2; LC/MS $t_{\text{R}} = 3.42$.

2-(4-(1H-Pyrazol-1-yl)phenyl)-2-acetamido-N-hydroxyacetamide (13a). 12a (120 mg, 0.44 mmol) was converted to the corresponding hydroxamic acid according to general procedure B. The reaction was complete after 30 min. After purification, 69 mg (57%) of off-white solid was obtained: ^1H NMR (DMSO) δ 11.01 (s, 1H), 9.01 (s, 1H), 8.69 (d, $J = 8.4$ Hz, 1H), 8.58–8.27 (m, 1H), 7.90–7.76 (m, 2H), 7.73 (d, $J = 1.4$ Hz, 1H), 7.49 (d, $J = 8.6$ Hz, 2H), 6.54 (dd, $J = 2.4/1.8$ Hz, 1H), 5.40 (d, $J = 8.4$ Hz, 1H), 1.91 (s, 3H); ^{13}C NMR (DMSO) δ 169.0, 166.6, 141.0, 139.1, 136.8, 128.1, 127.8, 118.3, 107.9, 53.2, 22.4; MS (TOF ES^+) m/z $\text{C}_{13}\text{H}_{15}\text{N}_4\text{O}_3$ $[\text{MH}]^+$ calcd 275.1, found 275.2; LC/MS $t_{\text{R}} = 3.07$.

N-(1-(4-(1H-Pyrazol-1-yl)phenyl)-2-(hydroxyamino)-2-oxoethyl)propionamide (13b). 12b (126 mg, 0.44 mmol) was converted to the corresponding hydroxamic acid according to general procedure B. The reaction was complete after 4 h. After purification, 44 mg (35%) of off-white solid was obtained: ^1H NMR (DMSO) δ 11.01 (d, $J = 1.2$ Hz, 1H), 9.02 (d, $J = 1.3$ Hz, 1H), 8.60 (d, $J = 8.4$ Hz, 1H), 8.47 (d, $J = 2.1$ Hz, 1H), 7.89–7.76 (m, 2H), 7.73 (d, $J = 1.5$ Hz, 1H), 7.50 (d, $J = 8.6$ Hz, 2H), 6.54 (dd, $J = 2.4/1.8$ Hz, 1H), 5.41 (d, $J = 8.4$ Hz, 1H), 2.22 (q, $J = 7.5$ Hz, 2H), 0.98 (t, $J = 7.6$ Hz, 3H); ^{13}C NMR (DMSO) δ 172.7, 166.6, 141.0, 139.0, 136.8, 128.1, 127.8, 118.3, 107.9, 53.1, 28.0, 9.83; MS (TOF ES^+) m/z $\text{C}_{14}\text{H}_{17}\text{N}_4\text{O}_3$ $[\text{MH}]^+$ calcd 289.1, found 289.2; LC/MS $t_{\text{R}} = 3.14$.

N-(1-(4-(1H-Pyrazol-1-yl)phenyl)-2-(hydroxyamino)-2-oxoethyl)isobutyramide (13c). 12c (122 mg, 0.40 mmol) was converted to the corresponding hydroxamic acid according to general procedure B. After 22 h of stirring, only partial conversion had occurred, so $\text{NH}_2\text{OH}\cdot\text{HCl}$ (70 mg, 1 mmol) and 5 M KOH/MeOH (0.5 mL, 2.5 mmol) were added, and stirring was continued at room temperature for a further 24 h. After purification, 71 mg (59%) of off-white solid was obtained: ^1H NMR (DMSO) δ 11.01 (d, $J = 1.2$ Hz, 1H), 9.03 (d, $J = 1.3$ Hz, 1H), 8.56 (d, $J = 8.5$ Hz, 1H), 8.51–8.43 (m, 1H), 7.88–7.77 (m, 2H), 7.73 (d, $J = 1.6$ Hz, 1H), 7.50 (d, $J = 8.6$ Hz, 2H), 6.54 (dd, $J = 2.4/1.8$ Hz, 1H), 5.40 (d, $J = 8.4$ Hz, 1H), 2.64 (hept, $J = 6.8$ Hz, 1H), 1.00 (d, $J = 6.8$ Hz, 3H), 0.97 (d, $J = 6.8$ Hz, 3H); ^{13}C NMR (DMSO) δ 175.9, 166.6, 141.0, 139.0, 136.9, 128.0, 127.8, 118.3, 107.9, 52.9, 33.3, 19.6, 19.5; MS (TOF ES^+) m/z $\text{C}_{15}\text{H}_{19}\text{N}_4\text{O}_3$ $[\text{MH}]^+$ calcd 303.1, found 303.2; LC/MS $t_{\text{R}} = 3.22$.

N-(1-(4-(1H-Pyrazol-1-yl)phenyl)-2-(hydroxyamino)-2-oxoethyl)pivalamide (13d). 12d (143 mg, 0.46 mmol) was converted to the corresponding hydroxamic acid according to general procedure B. After 22 h of stirring, only partial conversion had occurred, so $\text{NH}_2\text{OH}\cdot\text{HCl}$ (70 mg, 1 mmol) and 5 M KOH/MeOH (0.5 mL, 2.5 mmol) were added, and stirring was continued at room temperature for a further 24 h. At this point additional $\text{NH}_2\text{OH}\cdot\text{HCl}$ (139 mg, 2 mmol) and 5 M KOH/MeOH (0.6 mL, 3.0 mmol) were added, and stirring was continued for a further 24 h. After purification, 100 mg (68%) of glassy solid was obtained: ^1H NMR (DMSO) δ 11.02 (s, 1H), 9.08 (s, 1H), 8.47 (d, $J = 2.4$ Hz, 1H), 7.84–7.75 (m, 2H), 7.73 (d, $J = 1.4$ Hz, 1H), 7.51 (d, $J = 8.6$ Hz, 2H), 6.74–6.38 (m, 1H), 5.41 (d, $J = 8.1$ Hz, 1H), 1.15 (s, $J = 8.2$ Hz, 9H); ^{13}C NMR (DMSO) δ 176.9, 166.6, 141.0, 139.0, 136.9, 127.9, 127.8, 118.3, 107.9, 53.2, 38.2, 27.2; MS (TOF ES^+) m/z $\text{C}_{16}\text{H}_{21}\text{N}_4\text{O}_3$ $[\text{MH}]^+$ calcd 317.2, found 317.2; LC/MS $t_{\text{R}} = 3.30$.

2-(4-(1H-Pyrazol-1-yl)phenyl)-2-(3-tert-butylureido)-N-hydroxyacetamide (13e). 12e (147 mg, 0.44 mmol) was converted to the corresponding hydroxamic acid according to general procedure B.

After 4.5 h, starting material had disappeared by LC/MS, with the formation of the desired product and corresponding carboxylic acid (hydrolysis product). After FCC purification (eluent MeOH/DCM, 0:100 to 10:90), the major product isolated was found to be 2-(4-(1H-pyrazol-1-yl)phenyl)-2-(3-tert-butylureido)acetic acid (44 mg, 32%). This was directly converted to the desired hydroxamic acid according to general procedure D using CDI (3 equiv), $\text{NH}_2\text{OH}\cdot\text{HCl}$ (4 equiv), and anhydrous THF (2 mL). After purification, 11 mg (8% based on ester, 24% based on acid) of off-white solid was obtained: ^1H NMR (DMSO) δ 11.00 (s, 1H), 9.00 (s, 1H), 8.45 (d, $J = 2.5$ Hz, 1H), 7.80 (d, $J = 8.6$ Hz, 2H), 7.73 (d, $J = 1.6$ Hz, 1H), 7.42 (d, $J = 8.6$ Hz, 2H), 6.65 (d, $J = 8.6$ Hz, 1H), 6.59–6.46 (m, 1H), 6.12 (s, 1H), 5.18 (d, $J = 8.6$ Hz, 1H), 1.20 (s, 9H); ^{13}C NMR (DMSO) δ 167.3, 156.2, 140.9, 138.9, 138.4, 127.7, 127.5, 118.3, 107.8, 53.3, 49.1, 29.2; MS (TOF ES^-) m/z $\text{C}_{16}\text{H}_{20}\text{N}_5\text{O}_3$ $[\text{M} - \text{H}]^-$ calcd 330.2, found 330.2; LC/MS $t_{\text{R}} = 3.32$.

N-(1-(4-(1H-Pyrazol-1-yl)phenyl)-2-(hydroxyamino)-2-oxoethyl)benzamide (13f). 12f (161 mg, 0.48 mmol) was converted to the corresponding hydroxamic acid according to general procedure B. After 22 h of stirring, only partial conversion had occurred, so $\text{NH}_2\text{OH}\cdot\text{HCl}$ (70 mg, 1 mmol) and 5 M KOH/MeOH (0.5 mL, 2.5 mmol) were added, and stirring was continued at room temperature for a further 24 h. At this point additional $\text{NH}_2\text{OH}\cdot\text{HCl}$ (139 mg, 2 mmol) and 5 M KOH/MeOH (0.6 mL, 3.0 mmol) were added, and stirring was continued for a further 24 h. After FCC purification (eluent MeOH/DCM, 0:100 to 10:90), the major product isolated was found to be 2-(4-(1H-pyrazol-1-yl)phenyl)-2-benzamidoacetic acid (99 mg, 65%). This was directly converted to the desired hydroxamic acid according to general procedure D using CDI (3 equiv), $\text{NH}_2\text{OH}\cdot\text{HCl}$ (4 equiv), and anhydrous THF (5 mL). After purification, 7 mg (4% based on ester, 7% based on acid) of off-white solid was obtained: ^1H NMR (MeOD) δ 8.23 (dd, $J = 2.5/0.4$ Hz, 1H), 7.92–7.85 (m, 2H), 7.81–7.70 (m, 3H), 7.68–7.61 (m, 2H), 7.60–7.51 (m, 1H), 7.51–7.41 (m, 2H), 6.53 (dd, $J = 2.5, 1.9$ Hz, 1H), 5.68 (s, 1H); ^{13}C NMR (MeOD) δ 169.9, 169.3, 142.3, 141.3, 137.2, 135.0, 133.0, 129.9, 129.6, 129.1, 128.7, 120.5, 108.9, 56.2; MS (TOF ES^+) m/z $\text{C}_{18}\text{H}_{17}\text{N}_4\text{O}_3$ $[\text{MH}]^+$ calcd 337.1, found 337.2; LC/MS $t_{\text{R}} = 3.30$.

N-(1-(4-(1H-Pyrazol-1-yl)phenyl)-2-(hydroxyamino)-2-oxoethyl)-2-fluorobenzamide (13g). 12g (168 mg, 0.48 mmol) was converted to the corresponding hydroxamic acid according to general procedure B. The reaction was complete after 2 h. After purification, 100 mg (59%) of off-white solid was obtained: ^1H NMR (DMSO) δ 11.12 (d, $J = 1.2$ Hz, 1H), 9.14 (d, $J = 1.3$ Hz, 1H), 8.90 (dd, $J = 7.9/4.0$ Hz, 1H), 8.54–8.39 (m, 1H), 7.91–7.77 (m, 2H), 7.74 (d, $J = 1.4$ Hz, 1H), 7.65 (ddd, $J = 7.7/7.7/1.8$ Hz, 1H), 7.62–7.49 (m, 3H), 7.35–7.24 (m, 2H), 6.54 (dd, $J = 2.4/1.8$ Hz, 1H), 5.58 (d, $J = 7.9$ Hz, 1H); ^{19}F NMR (376 MHz, DMSO) δ –113.8; ^{13}C NMR (DMSO) δ 166.2, 163.1, 159.3 (d, $J_{\text{CF}} = 205.6$ Hz), 141.0, 139.2, 136.3, 132.9 (d, $J_{\text{CF}} = 8.5$ Hz), 130.4 (d, $J_{\text{CF}} = 2.6$ Hz), 128.2, 127.8, 124.5 (d, $J_{\text{CF}} = 3.3$ Hz), 121.7 (d, $J_{\text{CF}} = 30.4$ Hz), 118.4, 116.1 (d, $J_{\text{CF}} = 22.8$ Hz), 107.9, 53.9; MS (TOF ES^-) m/z $\text{C}_{18}\text{H}_{14}\text{FN}_4\text{O}_3$ $[\text{M} - \text{H}]^-$ calcd 353.1, found 353.1; LC/MS $t_{\text{R}} = 3.41$.

N-(1-(4-(1H-Pyrazol-1-yl)phenyl)-2-(hydroxyamino)-2-oxoethyl)-3-fluorobenzamide (13h). 12h (172 mg, 0.49 mmol) was converted to the corresponding hydroxamic acid according to general procedure B. The reaction was complete after 2 h. After purification, 101 mg (58%) of off-white solid was obtained: ^1H NMR (DMSO) δ 11.06 (d, $J = 1.2$ Hz, 1H), 9.11 (d, $J = 8.0$ Hz, 1H), 9.06 (d, $J = 1.3$ Hz, 1H), 8.53–8.44 (m, 1H), 7.88–7.81 (m, 2H), 7.81–7.71 (m, 3H), 7.61 (d, $J = 8.6$ Hz, 2H), 7.52 (ddd, $J = 8.1/8.1/6.1$ Hz, 1H), 7.45–7.35 (m, 1H), 6.55 (dd, $J = 2.4/1.8$ Hz, 1H), 5.63 (d, $J = 8.0$ Hz, 1H); ^{19}F NMR (376 MHz, DMSO) δ –113.1; ^{13}C NMR (DMSO) δ 166.4, 165.0, 164.2 (d, $J_{\text{CF}} = 225.0$ Hz), 141.0, 139.2, 136.1 (d, $J_{\text{CF}} = 6.9$ Hz), 136.0, 130.3 (d, $J_{\text{CF}} = 7.8$ Hz), 128.7, 127.8, 124.0 (d, $J_{\text{CF}} = 2.5$ Hz), 118.4 (d, $J_{\text{CF}} = 21.3$ Hz), 118.2, 114.6 (d, $J_{\text{CF}} = 23.1$ Hz), 107.9, 54.3; MS (TOF ES^+) m/z $\text{C}_{18}\text{H}_{16}\text{FN}_4\text{O}_3$ $[\text{MH}]^+$ calcd 355.1, found 355.2; LC/MS $t_{\text{R}} = 3.35$.

N-(1-(4-(1H-Pyrazol-1-yl)phenyl)-2-(hydroxyamino)-2-oxoethyl)-4-fluorobenzamide (13i). 12i (193 mg, 0.55 mmol) was converted to

the corresponding hydroxamic acid according to general procedure B. The reaction was complete after overnight stirring. After purification, 97 mg (50%) of off-white solid was obtained: ^1H NMR (DMSO) δ 11.05 (s, 1H), 9.05 (s, 1H), 9.02 (d, J = 8.1 Hz, 1H), 8.49 (d, J = 2.3 Hz, 1H), 8.09–7.90 (m, 2H), 7.83 (d, J = 8.7 Hz, 2H), 7.74 (d, J = 1.5 Hz, 1H), 7.61 (d, J = 8.6 Hz, 2H), 7.36–7.23 (m, 2H), 6.63–6.47 (m, 1H), 5.63 (d, J = 8.0 Hz, 1H); ^{19}F NMR (376 MHz, DMSO) δ –109.1; ^{13}C NMR (DMSO) δ 167.0 (d, J_{CF} = 230.6 Hz), 166.5, 165.3, 141.0, 139.2, 136.2, 130.5 (d, J_{CF} = 8.9 Hz), 130.3, 128.6, 127.8, 118.2, 115.1 (d, J_{CF} = 21.7 Hz), 108.1–107.6 (m), 54.3; MS (TOF ES⁺) m/z $\text{C}_{18}\text{H}_{16}\text{FN}_4\text{O}_3$ [MH]⁺ calcd 355.1, found 355.2; LC/MS t_{R} = 3.36.

N-(1-(4-(1*H*-Pyrazol-1-yl)phenyl)-2-(hydroxyamino)-2-oxoethyl)-3-aminobenzamide (**13l**). **12l** (121 mg, 0.35 mmol) was converted to the corresponding hydroxamic acid according to general procedure C to give 58 mg (47%) of off-white solid: ^1H NMR (DMSO) δ 11.03 (d, J = 0.9 Hz, 1H), 9.06 (d, J = 1.2 Hz, 1H), 8.53 (d, J = 8.1 Hz, 1H), 8.48 (d, J = 2.4 Hz, 1H), 7.82 (d, J = 8.7 Hz, 2H), 7.74 (d, J = 1.5 Hz, 1H), 7.60 (d, J = 8.6 Hz, 2H), 7.17–6.91 (m, 3H), 6.70 (ddd, J = 7.6/2.2/1.2 Hz, 1H), 6.62–6.45 (m, 1H), 5.59 (d, J = 8.1 Hz, 1H), 5.25 (s, 2H); ^{13}C NMR (DMSO) δ 166.8, 166.6, 148.7, 141.0, 139.1, 136.5, 134.6, 128.7, 128.4, 127.8, 118.3, 116.7, 114.8, 113.0, 107.9, 53.9; MS (TOF ES⁺) m/z $\text{C}_{18}\text{H}_{18}\text{N}_5\text{O}_3$ [MH]⁺ calcd 352.1, found 352.2; LC/MS t_{R} = 3.14.

N-(1-(4-(1*H*-Pyrazol-1-yl)phenyl)-2-(hydroxyamino)-2-oxoethyl)-4-aminobenzamide (**13m**). **12m** (46 mg, 0.13 mmol) was converted to the corresponding hydroxamic acid according to general procedure C to give 20 mg (43%) of off-white solid: ^1H NMR (DMSO) δ 11.01 (s, 1H), 9.02 (s, 1H), 8.48 (d, J = 2.2 Hz, 1H), 8.31 (d, J = 8.2 Hz, 1H), 7.81 (d, J = 8.7 Hz, 2H), 7.73 (d, J = 1.5 Hz, 1H), 7.66 (d, J = 8.7 Hz, 2H), 7.59 (d, J = 8.6 Hz, 2H), 6.65–6.39 (m, 3H), 5.67 (s, 2H), 5.60 (d, J = 8.2 Hz, 1H); ^{13}C NMR (DMSO) δ 166.9, 166.0, 152.0, 141.0, 139.1, 136.8, 129.3, 128.5, 127.8, 120.2, 118.2, 112.5, 107.9, 53.8; MS (TOF ES[−]) m/z $\text{C}_{18}\text{H}_{16}\text{N}_5\text{O}_3$ [M – H][−] calcd 350.1, found 350.1; LC/MS t_{R} = 3.19.

Biochemistry. Preparation of Recombinant MAPs. The production of recombinant malaria aminopeptidases in *Escherichia coli* and purification using a two-step purification process with a Ni–NTA–agarose column followed by size exclusion chromatography on a Superdex 200 16/60 column using an AKTExpress high-throughput chromatography system (<http://proteinexpress.med.monash.edu.au/index.htm>) was as described.^{7,9} Biochemical analysis indicated that the kinetic parameters (k_{cat} , K_m , k_{cat}/K_m) of material purified and used in subsequent crystallization trials were the same as published.^{7,9}

Enzymatic Analysis. The aminopeptidase activity of enzymes was determined by measuring the release of the fluorogenic leaving group, NHMec, from the fluorogenic peptide L-leucine-7-amido-4-methylcoumarin hydrochloride (H-Leu-NHMec) (Sigma L2145). The assay protocol devised by Stack et al. was modified and used.⁵ The reactions were carried out in 96-well microtiter plates, with a 200 μL total volume at 37 °C, using a spectrofluorimeter (BMG FLUOstar) with excitation at 355 nm and emission at 460 nm. PfA-M1 was preincubated in 100 mM Tris (pH 8.0) at 37 °C and PfA-M17 in 50 mM Tris (pH 8.0) and 2 mM CoCl₂ with the inhibitors for 10 min prior to the addition of substrate. Inhibitor concentrations were assayed between 0 and 500 μM . The fluorescence signal was monitored until a final steady-state velocity, V , was obtained. The K_i values were then evaluated using Dixon plots of $1/V$ versus inhibitor concentration while the substrate concentration was maintained lower than that of the K_m of the enzyme.

Crystallization and X-ray Data Collection. Crystals of the PfA-M1-bound complexes were obtained by cocrystallization of each compound with PfA-M1 in mother liquor containing 1 mM ligand. For PfA-M17-bound complexes, prior to data collection, crystals were soaked in mother liquor containing 1 mM ligand and 1 mM ZnSO₄. Data were collected at 100 K using synchrotron radiation at the Australian Synchrotron using the macromicrocrystallography MX1 beamline 3BM1 for PfA-M1 and the microcrystallography MX2 beamline 3ID1 for PfA-M17. Diffraction images were processed using iMosflm,⁵⁵ XDS,⁵⁶ pointless,^{57,58} and SCALA⁵⁷ from the CCP4 suite.⁵⁹ A total of 5% of each data set was flagged for calculation of R_{free} ⁶⁰ with neither a

σ nor a low-resolution cutoff applied to the data. A summary of statistics is provided in Supplementary Table 1 (Supporting Information). Subsequent crystallographic and structural analysis was performed using the Phenix suite.^{61,62} The inhibitor complex was initially solved and refined against the unbound PfA-M1 and PfA-M17 structures (protein atoms only) as described previously^{7,9,13,63,64} and clearly showed unbiased features in the active site for each structure. The coordinates and structure factors are available from the Protein Data Bank (PDB accession codes 4RST, 4RSV, 4RSX, 4R6T, 4R76, and 4R7M). Raw data and images are available from TARDIS (<https://store.synchrotron.org.au>).^{65,66}

Molecular Docking. Molecular docking was carried out by means of Molegro Virtual Docker (MVD) software (CLCbio). Ligands were built and energy minimized by using the PRODRG server.⁶⁷ Flexible torsions were automatically detected by MVD and manually checked for consistency. The obtained three-dimensional structures of PfA-M1 and PfA-M17 were prepared by automatically assigning bond orders and hybridization and adding explicit hydrogens, charges, and Tripos atom types. Missing heavy atoms were fixed by modeling them using Modeler v.9.8⁶⁸ and PyMod.⁶⁹ A search space of 12 Å radius, centered on 7, was used for docking. Side chain flexibility and displaceable waters were set for atoms at 5 Å or less from 7. The hydroxamic acid and NH of the Boc group of 7 were taken as electrostatic pharmacophoric groups for template-based dockings. In this way, if an atom of the ligand matches a group definition (e.g., positively/negatively charged), it is rewarded by using a weighted score (w) that depends on its distance to the group centers by using the following Gaussian function for each center:

$$w = \omega \exp(-d^2/r_0^2) \quad (1)$$

where d is the distance (Å) from the position of the atom to the center in the group, ω is a weight factor for the template group, and r_0 is a distance parameter specifying a characteristic distance for the template group. ω and r_0 were set at 2 and 1.80, respectively. An overall normalization of the similarity score term, to balance it with other scoring terms, was then applied for each atom. The grid-based MolDock score⁷⁰ with a grid resolution of 0.30 Å was used as the scoring function for docking. MolDock SE was used as the docking algorithm. For each ligand, 10 runs were defined. Similar poses (RMSD < 1.2 Å) were clustered, and the best scoring one was taken as representative. Other docking parameters were fixed at their default values. After docking, energy optimization of hydrogen bonds was performed.

Biology. *P. falciparum* Culture. An in vitro parasite culture of the *P. falciparum* strain 3D7 was maintained in RPMI with 10 mM Hepes (Life Technologies), 50 $\mu\text{g}/\text{mL}$ hypoxanthine (Sigma), and 5 mg/mL AlbuMAX II (Life Technologies). Human 0+ erythrocytes were obtained from the Australian Red Cross Blood Service (Agreement No. 13-04QLD-09). The parasites were maintained at 2–8% parasitemia at 5% hematocrit and incubated at 37 °C, 5% CO₂, 5% O₂, 90% N₂, and 95% humidity.

***P. falciparum* Growth Inhibition Assay.** A well-established *P. falciparum* imaging assay was used to assess parasite growth inhibition.⁴⁷ In brief, sorbitol (5%, w/v) synchronization was performed twice, approximately 8 h apart, on each synchronization day for two consecutive ring cycles, i.e., on days 1 and 3 of assay preparation. On day 2 the culture was split to approximately 2% trophozoite parasitemia. On day 4 the culture was split to 1–1.5% trophozoite parasitemia, which yielded approximately 8% ring parasitemia after 48 h on day 5, the day of the assay setup.

Compound stocks (10 mM in 100% DMSO) were diluted 1:25 in sterile water less than 24 h prior to use. An additional 1:10 dilution was performed, resulting in a 1:250 overall compound dilution and a final DMSO concentration of 0.4%. For dose response curves a three-step logarithmic serial dilution in 4% DMSO was prepared at 40 μM top concentration for test compounds and 2 μM for the positive control, artemisinin. A 5 μL volume of the diluted test compound or control solutions (20 μM artemisinin as the positive control and 4% DMSO as the negative control) were added to 384-well CellCarrier

imaging plates (PerkinElmer) for a final 1:10 dilution in parasite culture. The resulting final DMSO concentration for all sample dilutions and controls was 0.4%.

The parasite culture was added to a final concentration of 2% parasitemia and 0.3% hematocrit. The plates were incubated for 72 h at 37 °C, 5% CO₂, and 95% humidity. On day 8 the permeabilization and nuclear staining buffer was prepared in PBS containing 10 μg/mL saponin, 0.01% Triton X, and 5 mM EDTA (all Sigma) and 0.5 μg/mL 4',6-diamidino-2-phenylindole (DAPI; Life Technologies).⁴⁷

The plates were incubated at rt overnight before confocal imaging on an Opera confocal imager (PerkinElmer) at 405 nm excitation with a 20× water objective. Automated primary image analysis was performed concurrent with the imaging process utilizing an Acapella software (PerkinElmer) script to determine the number of parasites on the basis of the object size and fluorescence intensity.⁴⁷ Determination of the percentage of growth compared to the controls (2 μM artemisinin as the positive control and 0.4% DMSO as the negative control) was performed in Microsoft Excel 2010. Statistical analysis including IC₅₀ determination and graphical output was performed in GraphPad Prism 5 using nonlinear regression variable-slope curve fitting.

HEK293 Viability Assay. To assess the cytotoxicity of the compounds in dose response, a resazurin-based assay was utilized to test for cell viability. In brief, HEK293 cells were grown in DMEM medium (Life Technologies) containing 10% fetal calf serum (FCS; Gibco). The cells were trypsinized, counted, and seeded at 2000 cells per well in 45 μL of medium in TC-treated 384-well plates (Falcon) and left to adhere overnight at 37 °C, 5% CO₂, and 95% humidity.

Test compounds were prepared as described above to give a top final test concentration of 40 μM 0.4% DMSO. The plates were incubated for 72 h at 37 °C, 5% CO₂, and 95% humidity, and then the medium was removed and replaced by 35 μL of 44 μM resazurin in DMEM without FCS. The plates were incubated for another 4–6 h at 37 °C, 5% CO₂, and 95% humidity before being read on an EnVision plate reader (PerkinElmer) using fluorescence excitation/emission settings of 530 nm/595 nm. Determination of the percentage of growth compared to the controls (40 μM puromycin as the positive control and 0.4% DMSO as the negative control) was performed in Microsoft Excel 2010. Statistical analysis including IC₅₀ determination and graphical output was performed in GraphPad Prism 5 using nonlinear regression variable-slope curve fitting.

■ ASSOCIATED CONTENT

Ⓢ Supporting Information

Figures detailing compound docking (interactions of each compound for each model generated), representative compound electron density in crystal structures, and additional compound overlays and table listing crystallographic data collection details and refinement statistics. This material is available free of charge via the Internet at <http://pubs.acs.org>.

Accession Codes

PDB IDs: 4R5T, 4R5V, 4R5X, 4R6T, 4R76, 4R7M.

■ AUTHOR INFORMATION

Corresponding Authors

*Phone: +61 (0)3 9903 9542. E-mail: Peter.Scammells@monash.edu.

*Phone: +61 (0)3 9902 9309. Fax: +61 (0)3 9902 9500. E-mail: Sheena.McGowan@monash.edu.

Author Contributions

#S.N.M. and N.D. contributed equally to this work.

Notes

The authors declare no competing financial interest.

■ ACKNOWLEDGMENTS

S.M. is an Australian Research Council (ARC) Future Fellow (Grant FT100100690). We thank the National Health and Medical Research Council (Project Grant 1063786 to S.M. and P.J.S.) and the ARC (Grant LP120200557 to V.M.A.) for funding support. C.R. was an Endeavour Fellowship recipient (Grant 4100-2014). This work was supported by the Foundation for Polish Science and a statutory activity subsidy from the Polish Ministry of Science and Higher Education for the Faculty of Chemistry at the Wrocław University of Technology (to M.D.). We thank the Australian Synchrotron (MX-1 and MX-2) and the beamline scientists for beamtime and for technical assistance. We thank the Monash Platforms (Protein Production and Crystallization) for technical assistance. We thank the Australian Red Cross Blood Service for the provision of human blood.

■ ABBREVIATIONS USED

CDI, carbonyldiimidazole; DIPEA, *N,N*-diisopropylethylamine; FCC, flash column chromatography; HCTU, *O*-(1*H*-6-chlorobenzotriazol-1-yl)-1,1,3,3-tetramethyluronium hexafluorophosphate; PE, petroleum spirits 40–60; TEA, triethylamine; ZBG, zinc-binding group

■ REFERENCES

- (1) Liu, J.; Istvan, E. S.; Gluzman, I. Y.; Gross, J.; Goldberg, D. E. *Plasmodium falciparum* ensures its amino acid supply with multiple acquisition pathways and redundant proteolytic enzyme systems. *Proc. Natl. Acad. Sci. U.S.A.* **2006**, *103*, 8840–8845.
- (2) Rosenthal, P. J. Hydrolysis of erythrocyte proteins by proteases of malaria parasites. *Curr. Opin. Hematol.* **2002**, *9*, 140–145.
- (3) Lew, V. L.; Macdonald, L.; Ginsburg, H.; Krugliak, M.; Tiffert, T. Excess haemoglobin digestion by malaria parasites: a strategy to prevent premature host cell lysis. *Blood Cells Mol. Dis.* **2004**, *32*, 353–359.
- (4) Klemba, M.; Gluzman, I.; Goldberg, D. E. A *Plasmodium falciparum* dipeptidyl aminopeptidase I participates in vacuolar hemoglobin degradation. *J. Biol. Chem.* **2004**, *279*, 43000–43007.
- (5) Stack, C. M.; Lowther, J.; Cunningham, E.; Donnelly, S.; Gardiner, D. L.; Trenholme, K. R.; Skinner-Adams, T. S.; Teuscher, F.; Grembecka, J.; Mucha, A.; Kafarski, P.; Lua, L.; Bell, A.; Dalton, J. P. Characterization of the *Plasmodium falciparum* M17 leucyl aminopeptidase. A protease involved in amino acid regulation with potential for antimalarial drug development. *J. Biol. Chem.* **2007**, *282*, 2069–2080.
- (6) McGowan, S. Working in concert: the metalloaminopeptidases from *Plasmodium falciparum*. *Curr. Opin. Struct. Biol.* **2013**, *23*, 828–835.
- (7) McGowan, S.; Porter, C. J.; Lowther, J.; Stack, C. M.; Golding, S. J.; Skinner-Adams, T. S.; Trenholme, K. R.; Teuscher, F.; Donnelly, S. M.; Grembecka, J.; Mucha, A.; Kafarski, P.; Degori, R.; Buckle, A. M.; Gardiner, D. L.; Whisstock, J. C.; Dalton, J. P. Structural basis for the inhibition of the essential *Plasmodium falciparum* M1 neutral aminopeptidase. *Proc. Natl. Acad. Sci. U.S.A.* **2009**, *106*, 2537–2542.
- (8) Skinner-Adams, T. S.; Lowther, J.; Teuscher, F.; Stack, C. M.; Grembecka, J.; Mucha, A.; Kafarski, P.; Trenholme, K. R.; Dalton, J. P.; Gardiner, D. L. Identification of phosphinate dipeptide analog inhibitors directed against the *Plasmodium falciparum* M17 leucine aminopeptidase as lead antimalarial compounds. *J. Med. Chem.* **2007**, *50*, 6024–6031.
- (9) McGowan, S.; Oellig, C. A.; Birru, W. A.; Caradoc-Davies, T. T.; Stack, C. M.; Lowther, J.; Skinner-Adams, T.; Mucha, A.; Kafarski, P.; Grembecka, J.; Trenholme, K. R.; Buckle, A. M.; Gardiner, D. L.; Dalton, J. P.; Whisstock, J. C. Structure of the *Plasmodium falciparum* M17 aminopeptidase and significance for the design of drugs targeting

the neutral exopeptidases. *Proc. Natl. Acad. Sci. U.S.A.* **2010**, *107*, 2449–2454.

(10) Deprez-Poulain, R.; Flipo, M.; Piveteau, C.; Leroux, F.; Dassonneville, S.; Florent, I.; Maes, L.; Cos, P.; Deprez, B. Structure–activity relationships and blood distribution of antiplasmodial aminopeptidase-1 inhibitors. *J. Med. Chem.* **2012**, *55*, 10909–10917.

(11) Flipo, M.; Beghyn, T.; Leroux, V.; Florent, I.; Deprez, B. P.; Deprez-Poulain, R. F. Novel selective inhibitors of the zinc plasmodial aminopeptidase PfA-M1 as potential antimalarial agents. *J. Med. Chem.* **2007**, *50*, 1322–1334.

(12) Flipo, M.; Florent, I.; Grellier, P.; Sergheraert, C.; Deprez-Poulain, R. Design, synthesis and antimalarial activity of novel, quinoline-based, zinc metallo-aminopeptidase inhibitors. *Bioorg. Med. Chem. Lett.* **2003**, *13*, 2659–2662.

(13) Kannan Sivaraman, K.; Paiardini, A.; Sienczyk, M.; Ruggeri, C.; Oellig, C. A.; Dalton, J. P.; Scammells, P. J.; Drag, M.; McGowan, S. Synthesis and structure–activity relationships of phosphonic arginine mimetics as inhibitors of the M1 and M17 aminopeptidases from *Plasmodium falciparum*. *J. Med. Chem.* **2013**, *56*, 5213–5217.

(14) Freedman, L. D.; Doak, G. O. The preparation and properties of phosphonic acids. *Chem. Rev.* **1957**, *57*, 479–523.

(15) Babine, R. E.; Bender, S. L. Molecular recognition of protein-ligand complexes: applications to drug design. *Chem. Rev.* **1997**, *97*, 1359–1472.

(16) Sang, Q.; Jin, Y.; Newcomer, R. G. Matrix metalloproteinase inhibitors as prospective agents for the prevention and treatment of cardiovascular and neoplastic diseases. *Curr. Top. Med. Chem.* **2006**, *6*, 289–316.

(17) Flipo, M.; Charton, J.; Hocine, A.; Dassonneville, S.; Deprez, B.; Deprez-Poulain, R. Hydroxamates: relationships between structure and plasma stability. *J. Med. Chem.* **2009**, *52*, 6790–6802.

(18) Mucha, A.; Drag, M.; Dalton, J. P.; Kafarski, P. Metallo-aminopeptidase inhibitors. *Biochimie* **2010**, *92*, 1509–1529.

(19) Taillefer, M.; Xia, N.; Ouali, A. Efficient iron/copper co-catalyzed arylation of nitrogen nucleophiles. *Angew. Chem., Int. Ed.* **2007**, *46*, 934–936.

(20) Swapna, K.; Murthy, S. N. Copper iodide as a recyclable catalyst for Buchwald N-arylation. *Eur. J. Org. Chem.* **2010**, *34*, 6678–6684.

(21) Correa, A.; Bolm, C. Ligand-free copper-catalyzed N-arylation of nitrogen nucleophiles. *Adv. Synth. Catal.* **2007**, *2673*–2676.

(22) Zou, B.; Yuan, Q.; Ma, D. Cascade coupling/cyclization process to N-substituted 1,3-dihydrobenzimidazol-2-ones. *Org. Lett.* **2007**, *9*, 4291–4294.

(23) Sreedhar, B.; Arundhathi, R.; Reddy, P. L.; Reddy, M. A.; Lakshmi Kantam, M. Cu-Al hydrotalcite: an efficient and reusable ligand-free catalyst for the coupling of aryl chlorides with aliphatic, aromatic, and N (H)-heterocyclic amines. *Synthesis* **2009**, 2517–2522.

(24) Tubaro, C.; Biffis, A.; Scattolin, E.; Basato, M. Efficient catalysis of Ullmann-type arylation reactions by a novel trinuclear copper(I) complex with a chelating tricarbene ligand. *Tetrahedron* **2008**, *64*, 4187–4195.

(25) Uk Son, S.; Kyu Park, I.; Park, J.; Hyeon, T. Synthesis of Cu₂O coated Cu nanoparticles and their successful applications to Ullmann-type amination coupling reactions of aryl chlorides. *Chem. Commun. (Cambridge, U.K.)* **2004**, 778–779.

(26) Li, L.; Zhu, L.; Chen, D.; Hu, X.; Wang, R. Use of acylhydrazine and acylhydrazone-type ligands to promote CuI-catalyzed C–N cross-coupling reactions of aryl bromides with N-heterocycles. *Eur. J. Org. Chem.* **2011**, *2011*, 2692–2696.

(27) Oshovsky, G. V.; Ouali, A.; Xia, N.; Zablocka, M.; Boéré, R. T.; Duhayon, C.; Taillefer, M.; Majoral, J. P. Thiazolyl phosphine ligands for copper-catalyzed arylation and vinylation of nucleophiles in organic and aqueous media. *Organometallics* **2008**, *27*, 5733–5736.

(28) Biffis, A.; Tubaro, C.; Scattolin, E.; Basato, M.; Papini, G.; Santini, C.; Alvarez, E.; Conejero, S. Trinuclear copper(I) complexes with tricarbene ligands: catalysis of C–N and C–C coupling reactions. *Dalton Trans.* **2009**, 7223–7229.

(29) Joseph, P.; Priyadarshini, S.; Kantam, M. L. Sulfonic acid containing cation-exchanger resin “INDION-770” and copper (I) salts: a novel reusable catalyst for N-arylation of NH-heterocycles with haloarenes. *Catal. Sci. Technol.* **2011**, 234–238.

(30) Chouhan, G.; Wang, D.; Alper, H. Magnetic nanoparticle-supported proline as a recyclable and recoverable ligand for the CuI catalyzed arylation of nitrogen nucleophiles. *Chem. Commun. (Cambridge, U.K.)* **2007**, 4809–4811.

(31) Cristau, H. J.; Cellier, P. P.; Spindler, J. F.; Taillefer, M. Mild conditions for copper-catalyzed N-arylation of pyrazoles. *Eur. J. Org. Chem.* **2004**, 695–709.

(32) Xu, Z.-L.; Li, H.-X.; Ren, Z.-G.; Du, W.-Y.; Xu, W.-C.; Lang, J.-P. Cu(OAc)₂·H₂O-catalyzed N-arylation of nitrogen-containing heterocycles. *Tetrahedron* **2011**, *67*, 5282–5288.

(33) Li, F.; Hor, T. S. A. Facile synthesis of nitrogen tetradentate ligands and their applications in CuI-catalyzed N-arylation and azide-alkyne cycloaddition. *Chem.—Eur. J.* **2009**, *15*, 10585–10592.

(34) Wadhwa, K.; Yang, C.; West, P. R.; Deming, K. C.; Chemburkar, S. R.; Reddy, R. E. Synthesis of arylglyoxylic acids and their collision-induced dissociation. *Synth. Commun.* **2013**, *38*, 4434–4444.

(35) Abdel-Magid, A. F.; Carson, K. G.; Harris, B. D. Reductive amination of aldehydes and ketones with sodium triacetoxyborohydride. Studies on direct and indirect reductive amination procedures. *J. Org. Chem.* **1996**, *61*, 3849–3862.

(36) Usachova, N.; Leitis, G.; Jirgensons, A.; Kalvinsh, I. Synthesis of hydroxamic acids by activation of carboxylic acids with *N,N'*-carbonyldiimidazole: exploring the efficiency of the method. *Synth. Commun.* **2013**, *40*, 927–935.

(37) Tufariello, J. J.; Winzenberg, K. A. Nitrene-based synthesis of the pyrrolizidine alkaloid croalbinecine. *Tetrahedron Lett.* **1986**, *27*, 1645–1648.

(38) Chowdhury, N.; Dasgupta, S.; Pradeep Singh, N. D. Photoinduced DNA cleavage by anthracene based hydroxamic acids. *Bioorg. Med. Chem. Lett.* **2012**, *22*, 4668–4671.

(39) Riva, E.; Gagliardi, S.; Mazzoni, C.; Passarella, D.; Rencurosi, A.; Vigo, D.; Martinelli, M. Efficient continuous flow synthesis of hydroxamic acids and suberoylanilide hydroxamic acid preparation. *J. Org. Chem.* **2013**, *74*, 3540–3543.

(40) Huang, Q.; Mao, J.; Wan, B.; Wang, Y.; Brun, R.; Franzblau, S. G.; Kozikowski, A. P. Searching for new cures for tuberculosis: design, synthesis, and biological evaluation of 2-methylbenzothiazoles. *J. Med. Chem.* **2013**, *52*, 6757–6767.

(41) Zmitek, J.; Verhnjak, K.; Urleb, U.; Kotnik, S. Synthesis of (+)-(S)-ibuproxam and preparation of some new complexes of racemic and (+)-(S)-ibuproxam with B-cyclodextrin and its derivatives. *Chirality* **1995**, *7*, 206–210.

(42) Watkins, C. J.; Romero Maria Rosario, M.; Finn, P. W.; Kalvinsh, I.; Loza, E.; Lolya, D.; Starchenkov, I.; Bokaldere, R. M.; Semenikhina, V.; Harris, C. J.; Duffy, J. E. S. Carbamic acid compounds comprising an ether linkage as HDAC inhibitors. Patent WO2002026703 A1, 2002.

(43) Liguori, A.; Sindona, G.; Romeo, G.; Uccella, N. Direct conversion of hydroxamic acids into nitriles. *Synthesis* **1987**, *1987*, 168–168.

(44) Massaro, A.; Mordini, A.; Reginato, G.; Russo, F.; Taddei, M. Microwave-assisted transformation of esters into hydroxamic acids. *Synthesis* **2007**, *2007*, 3201–3204.

(45) Sivaraman, K. K.; Oellig, C. A.; Huynh, K.; Atkinson, S. C.; Poreba, M.; Perugini, M. A.; Trenholme, K. R.; Gardiner, D. L.; Salvesen, G.; Drag, M.; Dalton, J. P.; Whisstock, J. C.; McGowan, S. X-ray crystal structure and specificity of the *Plasmodium falciparum* malaria aminopeptidase PfM18AAP. *J. Mol. Biol.* **2012**, *422*, 495–507.

(46) Poreba, M.; McGowan, S.; Skinner-Adams, T.; Trenholme, K. R.; Gardiner, D. L.; Whisstock, J. C.; To, J.; Salvesen, G. S.; Drag, M.; Dalton, J. P. Fingerprinting the substrate specificity of M1 and M17 neutral aminopeptidases of human malaria, *Plasmodium falciparum*. *PLoS One* **2012**, *2*, e31938.

- (47) Duffy, S.; Avery, V. M. Development and optimization of a novel 384-well anti-malarial imaging assay validated for high-throughput screening. *Am. J. Trop. Med. Hyg.* **2012**, *86*, 84–92.
- (48) Lee, J.; Shim, J. S.; Jung, S. A.; Lee, S. T.; Kwon, H. J. N-Hydroxy-2-(naphthalene-2-ylsulfanyl)-acetamide, a novel hydroxamic acid-based inhibitor of aminopeptidase N and its anti-angiogenic activity. *Bioorg. Med. Chem. Lett.* **2005**, *15*, 181–183.
- (49) Wickstrom, M.; Larsson, R.; Nygren, P.; Gullbo, J.; Aminopeptidase, N. (CD13) as a target for cancer chemotherapy. *Cancer Sci.* **2011**, *102*, 501–508.
- (50) Hitzerd, S. M.; Verbrugge, S. E.; Ossenkoppele, G.; Jansen, G.; Peters, G. J. Positioning of aminopeptidase inhibitors in next generation cancer therapy. *Amino Acids* **2014**, *46*, 793–808.
- (51) Changklungmoa, N.; Chaithirayanon, K.; Kueakhai, P.; Meemon, K.; Riengrojpitak, S.; Sobhon, P. Molecular cloning and characterization of leucine aminopeptidase from *Fasciola gigantica*. *Exp. Parasitol.* **2012**, *131*, 283–291.
- (52) Didier, E. S.; Maddry, J. A.; Brindley, P. J.; Stovall, M. E.; Didier, P. J. Therapeutic strategies for human microsporidia infections. *Expert Rev. Anti-Infect. Ther.* **2005**, *3*, 419–434.
- (53) Carroll, R. K.; Veillard, F.; Gagne, D. T.; Lindenmuth, J. M.; Poreba, M.; Drag, M.; Potempa, J.; Shaw, L. N. The *Staphylococcus aureus* leucine aminopeptidase is localized to the bacterial cytosol and demonstrates a broad substrate range that extends beyond leucine. *Biol. Chem.* **2013**, *394*, 791–803.
- (54) Dong, L.; Cheng, N.; Wang, M. W.; Zhang, J.; Shu, C.; Zhu, D. X. The leucyl aminopeptidase from *Helicobacter pylori* is an allosteric enzyme. *Microbiology* **2005**, *151*, 2017–2023.
- (55) Batty, T. G.; Kontogiannis, L.; Johnson, O.; Powell, H. R.; AG, L. iMOSFLM: a new graphical interface for diffraction-image processing with MOSFLM. *Acta Crystallogr., D: Biol. Crystallogr.* **2011**, *67*, 271–281.
- (56) Kabsch, W. XDS. *Acta Crystallogr., D: Biol. Crystallogr.* **2010**, *66*, 125–132.
- (57) Evans, P. Scaling and assessment of data quality. *Acta Crystallogr., D: Biol. Crystallogr.* **2006**, *62*, 72–82.
- (58) Evans, P. R. An introduction to data reduction: space-group determination, scaling and intensity statistics. *Acta Crystallogr., D: Biol. Crystallogr.* **2011**, *67*, 282–292.
- (59) CCP4. The CCP4 suite: programs for protein crystallography. *Acta Crystallogr., D: Biol. Crystallogr.* **1994**, *DS0*, 760–763.
- (60) Brunger, A. T. Assessment of phase accuracy by cross validation: the free R value. Methods and applications. *Acta Crystallogr., D: Biol. Crystallogr.* **1993**, *49*, 24–36.
- (61) Adams, P. D.; Afonine, P. V.; Bunkóczi, G.; Chen, V. B.; Davis, I. W.; Echols, N.; Headd, J. J.; Hung, L.-W.; Kapral, G. J.; Grosse-Kunstleve, R. W.; McCoy, A. J.; Moriarty, N. W.; Oeffner, R.; Read, R. J.; Richardson, D. C.; Richardson, J. S.; Terwilliger, T. C.; Zwart, P. H. PHENIX: a comprehensive Python-based system for macromolecular structure solution. *Acta Crystallogr., D: Biol. Crystallogr.* **2010**, *D66*, 213–221.
- (62) Afonine, P. V.; Grosse-Kunstleve, R. W.; Echols, N.; Headd, J. J.; Moriarty, N. W.; Mustyakimov, M.; Terwilliger, T. C.; Urzhumtsev, A.; Zwart, P. H.; Adams, P. D. Towards automated crystallographic structure refinement with phenix.refine. *Acta Crystallogr., D: Biol. Crystallogr.* **2012**, *D68*, 352–367.
- (63) Harbut, M. B.; Velmourougane, G.; Dalal, S.; Reiss, G.; Whisstock, J. C.; Onder, O.; Brisson, D.; McGowan, S.; Klemba, M.; Greenbaum, D. C. Bestatin-based chemical biology strategy reveals distinct roles for malaria M1- and M17-family aminopeptidases. *Proc. Natl. Acad. Sci. U.S.A.* **2011**, *108*, E526–E534.
- (64) Velmourougane, G.; Harbut, M. B.; Dalal, S.; McGowan, S.; Oellig, C. A.; Meinhardt, N.; Whisstock, J. C.; Klemba, M.; Greenbaum, D. C. Synthesis of new (–)-bestatin-based inhibitor libraries reveals a novel binding mode in the S1 pocket of the essential malaria M1 metalloaminopeptidase. *J. Med. Chem.* **2011**, *54*, 1655–1666.
- (65) Androulakis, S.; Schmidberger, J.; Bate, M. A.; DeGori, R.; Beitz, A.; Keong, C.; Cameron, B.; McGowan, S.; Porter, C. J.; Harrison, A.; Hunter, J.; Martin, J. L.; Kobe, B.; Dobson, R. C.; Parker, M. W.; Whisstock, J. C.; Gray, J.; Treloar, A.; Groenewegen, D.; Dickson, N.; Buckle, A. M. Federated repositories of X-ray diffraction images. *Acta Crystallogr., D: Biol. Crystallogr.* **2008**, *D64*, 810–814.
- (66) Meyer, G. R.; Aragao, D.; Mudie, N. J.; Caradoc-Davies, T. T.; McGowan, S.; Bertling, P. J.; Groenewegen, D.; Quenette, S. M.; Bond, C. S.; Buckle, A. M.; Androulakis, S. Operation of the Australian Synchrotron for macromolecular crystallography. *Acta Crystallogr., D: Biol. Crystallogr.* **2014**, *D70*, 2510–2519.
- (67) Schüttelkopf, A. W.; van Aalten, D. M. F. PRODRG: a tool for high-throughput crystallography of protein-ligand complexes. *Acta Crystallogr., D: Biol. Crystallogr.* **2004**, *D60*, 1355–1363.
- (68) Eswar, N.; Eramian, D.; Webb, B.; Shen, M.; Sali, A. Protein structure modeling with MODELLER. *Methods Mol. Biol.* **2008**, *426*, 145–159.
- (69) Bramucci, E.; Paiardini, A.; Bossa, F.; Pascarella, S. PyMod: sequence similarity searches, multiple sequence-structure alignments, and homology modeling within PyMOL. *BMC Bioinf.* **2012**, *13* (Suppl. 4), S2.
- (70) Thomsen, R.; Christensen, M. MolDock: a new technique for high-accuracy molecular docking. *J. Med. Chem.* **2006**, *49*, 3315–3321.